




RESEARCH ARTICLE

WILEY

Some evolutionary patterns of palaeokarst developed in Pleistocene deposits (Ebro Basin, NE Spain): Improving geohazard awareness in present-day karst

María Asunción Soriano¹  | Andrés Pocoví¹ | Héctor Gil² | Antonio Pérez¹ | Aránzazu Luzón¹ | Miguel Ángel Marazuela^{3,4,5}

¹Grupo Geotransfer, Departamento de Ciencias de la Tierra, Facultad de Ciencias, Instituto de Investigación en Ciencias Ambientales (IUCA), Universidad de Zaragoza, Zaragoza, Spain

²Departamento de Ciencias de la Tierra, Universidad de Zaragoza, Zaragoza, Spain

³Institute of Environmental Assessment and Water Research (IDAEA), CSIC, Barcelona, Spain

⁴Department of Civil and Environmental Engineering, Universidad Politécnica de Cataluña (UPC), Barcelona, Spain

⁵Associated Unit: Hydrogeology Group, UPC-CSIC, Barcelona, Spain

Correspondence

María Asunción Soriano, Departamento de Ciencias de la Tierra, Facultad de Ciencias, Instituto de Investigación en Ciencias Ambientales (IUCA), Universidad de Zaragoza, Pedro Cerbuna 12, 50009 Zaragoza, Spain. Email: asuncion@unizar.es

Handling Editor: I. D. Somerville

Pleistocene detrital deposits in the central Ebro Basin frequently show deformation features due mainly to karstification in the underlying Neogene evaporites. In 123 cases, estimation of parameters of shape and minimum volume of materials involved was accomplished. Six of them were analysed in more detail to establish the main processes involved in their genesis and the succession of events. All the deformation features in the selected sites are synsedimentary. To achieve the objectives, intense fieldwork was made applying methods of sedimentology and structural geology. Usually, a complex evolutionary pattern was observed, with evidences of dissolution, sagging, collapse, gravity flow, suffosion, and plastic flow. In a schematic way, three main situations, independent of the age of the analysed deposits, can be distinguished: (a) slow subsidence, (b) collapse, and (c) temporal overlapping of both processes. In the first 2 scenarios, basins with smooth or abrupt borders, respectively, were generated on the land surface. In the third one, slow subsidence was followed by a collapse, located in the area of maximum flexure. These patterns are also observed in present-day dolines. Comparison of direct and indirect parameters between paleodolines and present-day dolines indicates a bigger size of the latter, probably caused by the different conditions of observation. This study helps to know the possibilities in the evolution of mantled karst features, to estimate the volume of material affected by karstification and to improve the knowledge of present-day dolines behaviour. Consequently, study of paleodolines must be considered to achieve a better urban planning in active karstic areas.

KEYWORDS

doline parameters estimation, evaporites, land-use planning, mantled karst, natural hazard, synsedimentary deformation features

1 | INTRODUCTION

Development of dolines with soil cover is a major geohazard related to karst because they may constitute small zones with very unstable ground, as Waltham, Bell, and Culshaw (2005) indicate. Different authors have considered that most of these landforms are inherited and induced or accelerated by man's activities (De Waele et al., 2017; Horwitz & Smith, 2003; Land & Asanidze, 2015; Mancini, Stecchi, Zanni, & Gabbianelli, 2009; Parise et al., 2015; Waltham, 2008; Waltham et al., 2005). Analysing hazards caused by karstification in mantled karst, that is, soluble rocks covered by unconsolidated sediments (Klimchouk, 2013), is not an easy task. Karst landforms are generated mainly by dissolution of soluble rocks and

dominant underground drainage. The hydraulic gradient and the properties of the involved rocks (lithology and structure) are determining factors in its development (Ford & Williams, 2007; Waltham et al., 2005; White, 1988; Williams, 2003). In addition, whenever mantled karst is considered, the behaviour of the detrital cover should be also taken into account (Ford, 1997). In these conditions, although dissolution is the main process in karst, others such as collapse, gravity, suffosion, and plastic flow can also be involved (Andrejchuk & Klimchouk, 2002; Beck, 1984; Beck & Pearson, 1995; Ford & Williams, 2007; Gutierrez, Guerrero, & Lucha, 2008; Waltham et al., 2005; White & White, 1969; Williams, 2003). At the surface, the most relevant landforms, consequence of these processes developed at depth, are dolines (sinkholes).

Palaeokarst refers to karst developed largely or entirely during past geological periods (Bosák, Ford, & Glazek, 1989). There are numerous examples of karstification in the geologic time (Decarlis & Lualdi, 2008; Ershova, Prokopiev, Khudoleya, & Fefilova, 2012; Evans & Reed, 2007; Fei et al., 2016; Khalaf, 2011). Economic, engineering, and scientific significance of palaeokarst is highlighted in several works (Bosák, 1989; Eraso, 1989; Min & Mao, 2002; Zhao, Shen, Qiao, Zheng, & Wang, 2014). In addition, palaeokarst studies could be used as analogue models in order to illustrate evolution patterns of present karst areas (Pueyo-Anchuela et al., 2014; Soriano et al., 2012). Numerous examples of palaeokarst are related to evaporites (Andrejchuk & Klimchouk, 2002; Columbu et al., 2015; Cooper & Waltham, 1999; Doğan & Özel, 2005; Eliassen & Talbot, 2005; Guerrero, Gutierrez, & Galve, 2013; Rodríguez-Aranda, Calvo, & Sanz-Montero, 2002; Silva et al., 2012; Smith & Goodknight, 2005; Soriano et al., 2012, and references therein).

In the central Ebro Basin, diapirism, tectonics, and mainly, karstification have generated deformation structures. Those are visible both in natural and man-made outcrops of Pleistocene sediments (mainly fluvial) that cover Neogene evaporites. The age of the affected deposits ranges from Early to Late Pleistocene (Julián Andrés & Chueca Cía, 1998; Gil et al., 2013; Gil Marín, Esnaola Gómez, Marqués, & Herranz, 1998; Marqués, Santos, Esnaola, & Gil, 1998; Soriano et al., 2012). Research on palaeokarst in this area has been focused on studying the influence of karst on sedimentation, application to develop a genetic classification of present dolines, comparison of karst effects in sediments with other processes, such as diapirism or tectonics, and so forth (Benito, Pérez-González, Gutierrez, & Machado, 1998; Benito, Sancho, Peña, Machado, & Rhodes, 2010; Gil, Luzón, et al., 2013; Gutiérrez et al., 2008; Gutiérrez, Parise, de Waele, & Jourde, 2014; Luzón, Pérez, Soriano, & Pocoví, 2008; Luzón et al., 2012; Simón et al., 2014). In addition, mantled karst is still today's one of the main geological processes observed in this region. It has been profusely studied (geomorphological, geophysics, geo-technical, and trenching aspects), because both high solubility of evaporites and heavy human presence in the karst area increase the risk (Soriano et al., 2012).

Some of the outcrops in this region provide a direct observation to the inner part of the paleodeformation structures. The knowledge that can be extracted is higher than that obtained with some of the previous methods mentioned, because they provide only indirect or more restricted data. The detailed study of such paleostructures considering structural, morphological, and sedimentological features of the materials affected by syndepositional karst indicates, in general, more complexity than at first expected. For this reason, this paper deals with the study of the evolution of some selected paleodeformation structures (six among the 123 cases observed) with the establishment of the involved genetic processes and, also, the succession of events. Its knowledge might help to better understand the behaviour of present dolines developed in mantled karst. In addition, the large number of studied cases permits to estimate the shape and the minimum total area and volume of materials affected by karstification, as well as to compare them with data of present-day dolines. This study could have a direct application in the mitigation of the exposure to this geohazard and help alert authorities and, consequently, propose more adequate

solutions to this environmental problem. This will, hopefully, be reflected in better land-use planning. The surroundings of Zaragoza are excellent to study these aspects because there are numerous examples of karst (old and present). In addition, this region is submitted to a high human pressure (rural, industrial, residential, and tertiary mixed land use, as Lamelas, 2007, has noted) with the following complexity of environmental sustainability. The results obtained can have a direct application in other similar scenarios. Moreover, in some of the examples described, sedimentological features were conditioned by syndepositional karst activity usually not considered when only a morphological study is achieved. For such reason, to obtain the previous goals, a multidisciplinary study has been carried out.

2 | GEOLOGICAL SETTING

The research area is located in the central zone of the Ebro Basin (Figure 1). An endorheic regime prevailed in this basin from the Late Eocene to the Late Miocene being disconnected from the Atlantic Ocean and the Mediterranean Sea by three topographic barriers: Pyrenees in the north, Catalanian Coastal Range in the east, and Iberian Range in the northwest-southeast (Arche, Evans, & Clavell, 2010; García-Castellanos, Vergés, Gaspar-Escribano, & Cloetingh, 2003; Muñoz et al., 2002). During the endorheic stage, alluvial fans spread from the margins and connected with freshwater or saline lakes in the central part of the basin (Muñoz et al., 2002; Pardo et al., 2004). Nowadays, the fluvial network is dominated by the southeast-flowing Ebro River and its tributaries that, in the study zone, are the Jalón, Huerva, and Gállego rivers (Figure 1). During the Quaternary, several terrace and pediment levels have been developed (Esnaola & Leyva, 1995; Gil Marín et al., 1998; Guerrero et al., 2013; Marqués et al., 1998; Soriano, 1990).

The exposed stratigraphic succession in the area is dominated by Miocene evaporite beds belonging to the Zaragoza Formation, which were deposited mainly in a wide salt pan. These rocks are disconformably covered by Quaternary fluvial and alluvial deposits corresponding to the recent exorheic basin stage that began during the Late Miocene (García-Castellanos et al., 2003). The Miocene succession is nearly horizontal or gently deformed by folds, joints, and faults (Arlegui & Simón, 2001; Quirantes, 1978). The observed structural discontinuities can be grouped into two main sets: (a) an N-S striking older set and (2) a NW-SE to E-W striking younger set that are the two main trends of the recent regional stress field in this region (Liesa & Simón, 2009). These dominant directions are visible on a regional scale as lineaments affecting both the Miocene and Quaternary materials (Arlegui & Soriano, 2003) and also at outcrop (Arlegui & Simón, 2000).

The Pleistocene succession is dominated by fluvial gravels, but other deposits such as aeolian sands, loess, alluvial breccias, or lacustrine mudstones also occur (Gil, Luzón, et al., 2013; Luzón et al., 2012) evidencing a complex paleogeographical framework (Figure 2), although a southeast-flowing fluvial system with braided channels and gravel bars dominated the scenery (Luzón et al., 2008). In the alluvial plain, small lakes locally developed in subsiding karst areas (Luzón et al., 2008), where small deltas grew when reached by flooding (Luzón

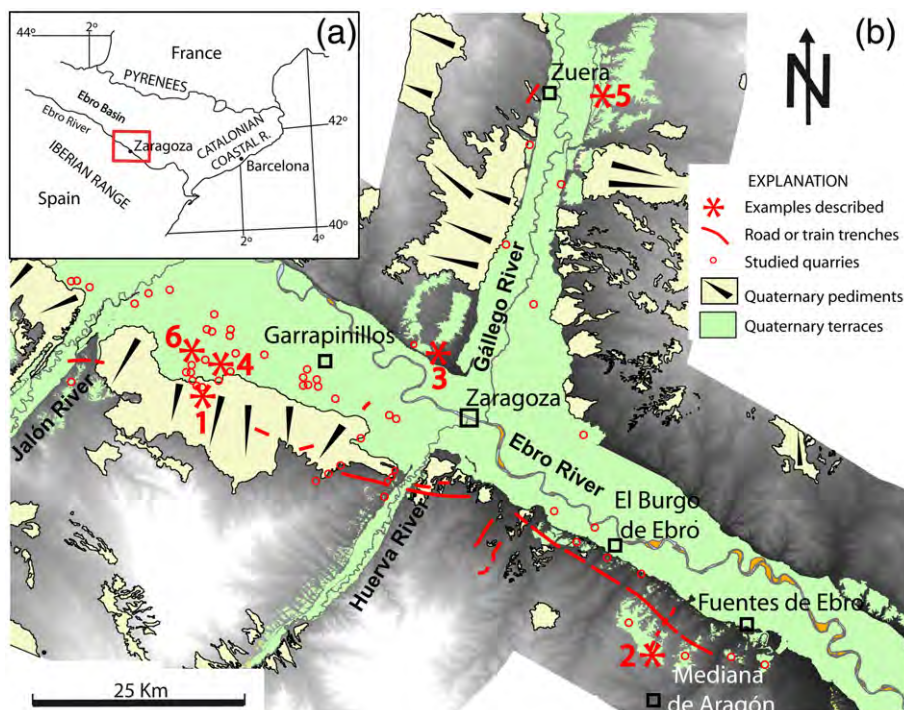
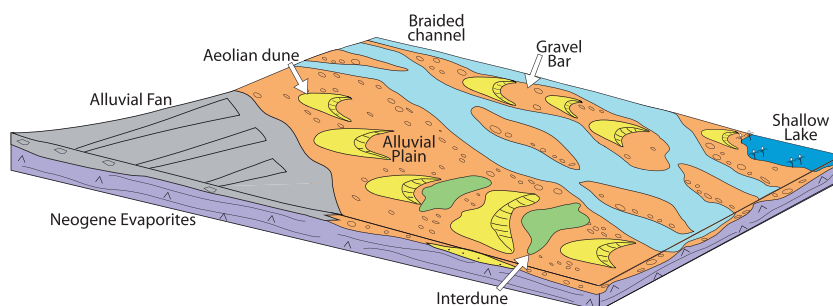


FIGURE 1 Location of the studied area: (a) geographical location in the NE of Spain. (b) Digital map showing the situation of the main Quaternary landforms, studied sites, and selected sites analysed in this paper [Colour figure can be viewed at wileyonlinelibrary.com]

FIGURE 2 Palaeogeographical sketch showing the main sedimentary environments developed in the central Ebro Basin during the Pleistocene [Colour figure can be viewed at wileyonlinelibrary.com]



et al., 2011; Pueyo-Anchuela et al., 2014). During episodes of low availability of water, alluvial plains were exposed, acting as source of sand for dunes generation (Luzón et al., 2012); the wind pattern was quite similar to the recent one and alluvial fans, fed in the nearby reliefs made on Neogene rocks, prograded (Gil, Luzón, et al., 2013).

This geological framework and the related deposits have favoured the development of a mantled karst in the region. Karst has been active since, at least, the Early Pleistocene (Gil, Luzón, et al., 2013) and a close examination of the Pleistocene succession evinces different shapes attributed to diverse types of dolines (Gutiérrez et al., 2008). Karstification has been the main cause for the preservation of erodible sediments, such as sand dunes and lacustrine muds in subsiding areas (Luzón et al., 2012; Simón et al., 2014). Dissolution has also caused aggradation of fluvial deposits, which locally show conspicuous thickness variations that reflect channel adjustments related to changes in the equilibrium profile of the rivers (Benito et al., 1998; Gil, Luzón, et al., 2013; Guerrero et al., 2008). Nowadays, karstification is still active, and dolines cause frequent damages in both urban and rural areas; they have been analysed from different aspects such as mapping, risk, and geophysical studies (Galve et al., 2009; Guerrero,

Gutiérrez, & Lucha, 2004; Gutiérrez-Santolalla, Gutiérrez-Elorza, Marín, Maldonado, & Younger, 2005; Lamelas, Marinoni, Hoppe, & de la Riva, 2008; Pueyo-Anchuela, Casas, Soriano, & Pocióvi, 2010; Pueyo-Anchuela, et al., 2015; Soriano et al., 2012; Soriano & Simón, 1995, 2002).

3 | METHODOLOGY

Urban expansion has increased in the last few decades in the central Ebro Basin causing plenty of civil works. Those and subsequent activities in quarries generated a high number of excellent artificial outcrops (up to 20 m in height) exposing Quaternary deposits belonging to terraces and pediments, mainly of Early and Late Pleistocene age where numerous deformation structures can be analysed.

After intense fieldwork, multiple survey lines were studied that cover 73 sites, and a total length of exposure estimated to be about 35 km (Figure 1). Among 123 examples studied, six have been selected for more detailed description, as they represent different dominating processes and have special peculiarities concerning their temporal

and spatial development, as well as to the relationships between the main acting processes. Some of these processes are also observed in present-day karst. The criteria followed for selection of sites included different age of deposits, quality and thickness of outcrops, and existence of diverse deformation structures (reflecting a variety of processes). Because, in many cases, the contact between Miocene rocks and Quaternary sediments is not exposed, data from drillings (Confederación Hidrográfica del Ebro, 2017) and isopach maps of Quaternary deposits (Lamelas, 2007; Simón, Soriano, Arlegui, & Caballero, 1998) were used as complementary tools.

The study of the inner characteristics of paleodeformation structures requires the utilization of sedimentology and structural geology methods, because the examples studied in more detail have been proved as synsedimentary deformations. In this way, exhaustive field surveys, detailed outcrop observations, elaboration of cross-sections, and sedimentological sketches were made. Lithofacies definition was the basis for interpretation of architectural elements, in the sense of Miall (1996); this permitted a better comprehension of the evolutionary history of each deformation structure. A particular emphasis was imputed to the identification of geometrical relationships among strata that have experienced synsedimentary deformation of currently several non-active structures. Whenever possible, structural analysis of the deformation structures was also made following a standard protocol: compilation of data on faults, joints and folds, projection on to equal-area stereoplots, and retrodeformational analysis to obtain a kinematical reconstruction of structures.

In addition, 123 examples of palaeodeformation structures were selected to determine an estimate of the area and of the minimum affected volume associating these structures with simple geometrical features (cones in the case of slow subsidence and cylinders in collapse) and their diverse relationships (see Figure 3). Direct measurements in the field and detailed photographs were utilized to determine the basic parameters (diameter and height) necessary to obtain this estimation. These are approximations by defect because (a) the observed height of outcrops usually does not reach the contact with evaporite rocks, (b) most of the analysed sections do not cut the central area of the deformation structure, and (c) the geometrical figure is a simplification of the real structure. Moreover, data obtained from paleostructures were compared with those of present dolines, as an exhaustive inventory of dolines located in the surroundings of Zaragoza exists (Simón et al., 1998). Volumetric data could not be compared because the depth parameter is not reflected in this inventory.

Outcrops of Neogene evaporites were also taken into consideration because they provide direct information to determine or corroborate the main processes being involved in the development of the analysed karst structures.

4 | RESULTS

After the observation of multiple outcrops, it is widely demonstrated that the Neogene evaporite rocks of the Ebro Basin are, in general, slightly deformed. Dissolution has been favoured in more soluble beds and fracture planes (Figure 4a,b). In sections with a high degree of karstification, usually, there are fragments of the evaporite rocks inside

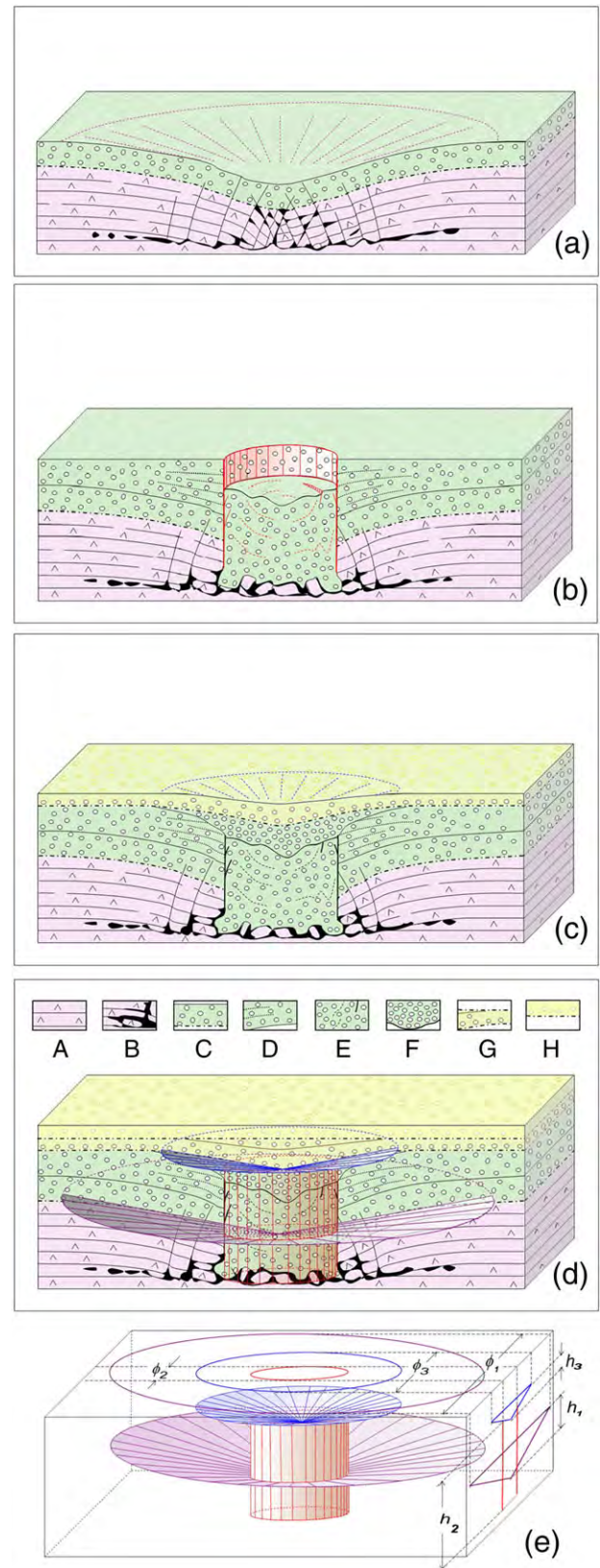


FIGURE 3 General (a to d) and idealized (e) schemas utilized to estimate by defect the area and volume affected by karst. Legends in (d): (A) Miocene evaporites; (B) karstified evaporites; (C) presubsidence Quaternary deposits; (D) synsubsidence “1” deposits; (E) collapse “2” deposits; (F) fallen deposits; (G) synsubsidence “3” deposits; (H) postsubsidence deposits. In (e): h = height and ϕ = diameter (1, 2, and 3 are the lower subsidence cone, collapse cylinder, and upper subsidence cone, respectively). [Colour figure can be viewed at wileyonlinelibrary.com]

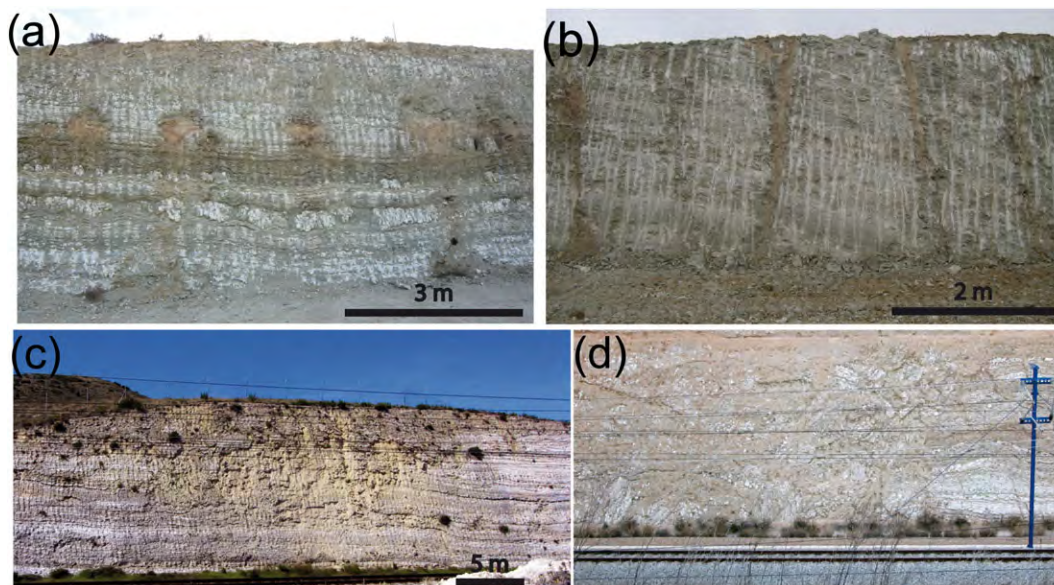


FIGURE 4 Diverse features affecting Neogene evaporites: (a) conduits in more soluble (glauberite rich) beds, SE Zaragoza. (b) Fractures facilitate dissolution, S of Zaragoza. (c) Lateral continuity of beds with and without karstification evidences, SE of El Burgo de Ebro. (d) High deformation in evaporites is marked by presence of fractures, bending of beds, fragments of rocks, karstic residuum, among others, SE of El Burgo de Ebro [Colour figure can be viewed at wileyonlinelibrary.com]

a matrix made of insoluble residue (karstic residuum according to Warren, 2006). In many cases, the lateral continuity of these levels with beds without dissolution is evident (Figure 4c). However, in others, dissolution of evaporites has been very important and the presence of voids, fractures, bended beds, and fragments of rocks has been observed (Figure 4d).

Paying attention to the main karst processes that affect Quaternary sediments, three simplified different scenarios are proposed. Two of them involve a more simple evolution, as there is clearly a dominating process (slow or fast subsidence), whereas the third one is more complex as both processes participate. The detailed study of six cases is used to expose the main characteristics, genetical processes, and deduced evolutionary stages. The location, age, and sedimentological characterization of the studied examples are summarized in Figure 1 and Table 1.

4.1 | Dominance of slow subsidence scenario

Two examples (1 and 2) developed in Middle and Early Pleistocene deposits, respectively, were studied (Figures 1, 5, and 6 and Table 1). Gravels dominate, with abundant mud (especially in Case 2) and rare interbedded sand (Figures 5 and 6). In Example 1, calcrete levels developed. The sedimentological characteristics indicate that the lower deposits of Example 1 and the upper ones of Example 2 generated in a dominated braided fluvial system. Gravels alternating with calcretes evidence episodic fluvial sedimentation and a water level close to the land surface during nonsedimentation episodes. Gravity flow deposits are related with supplies from lateral alluvial fans. Marls with calcretes (Figure 6) are interpreted as palustrine facies (Luzón et al., 2011; Pueyo-Anchuela et al., 2014). Neogene evaporites and marls can be identified in the lower part of Example 2 (Figure 6).

In both examples, beds are tilted towards the centre of the paleostructure drawing a basin section. Lateral variations in thickness

of beds and unconformities can be clearly observed. In addition, Example 2 (Figure 6) is clearly asymmetric. In the central part of the structure, there is a conduit filled with mud and gravel, which have been dragged downwards, affecting the base of the Pleistocene deposits. Numerous faults (normal and reverse) cut mainly the lower marl levels. They are nearly vertical, with main NW-SE and minor NNW-SSE striking surfaces dipping both to the north and south (Figure 6b). Folds verging towards the central part of the synform and shear bands (with disorganized gravels even showing vertical A-axis that demonstrate deformation after deposition) are observed, and in the southern side, the upper gravel beds are even displaced.

The detailed interpretation of evolutionary stages of Example 1 is shown in Figure 5b. In summary, the dissolution of the Neogene evaporites conditioned the deformation of the Quaternary deposits where several episodes of slow subsidence can be inferred. In short, Example 2 was mainly generated by successive dissolution-slow subsidence episodes. To a much lesser extent, suffosion and collapse processes collaborated in the final arrangement of these deposits.

4.2 | Dominance of collapse scenario

Two cases (Examples 3 and 4) in Early and Late Pleistocene deposits were selected (see Figures 1, 7a, and 8a). Gravels dominate with minor sand and mud levels (see Table 1 for details). The facies features indicate fluvial sedimentation, with dominating longitudinal gravel bars and braided channels. In Example 3, presence of several fining-upward sequences evidences changes in sedimentation, with the active fluvial areas being substituted by flooding zones. Intense deformation is observed in the lower gravel units whereas no deformation exists in the upper ones. In Example 4, the lowermost unit locally includes sandy bedforms generated during low discharge periods and, also, a U-shaped mudstone body that represents local ponding (Luzón et al., 2008).

TABLE 1 Lithofacies present in each of the examples described

Sedimentary setting and architectural elements	Lithofacies
<p>1. Terrace T4 Ebro R. +70 m (Soriano, 1990). Middle Pleistocene (Marqués et al., 1998)</p> <p>Fluvial system. Longitudinal bars (GB), braided channels, and very occasional noncohesive gravity flows (SG2)</p> <p>Alluvial plain. Calcretes (C)</p> <p>Alluvial fans. Cohesive gravity flow deposits (SG1), braided channels (CH), and floodplain fines (FF)</p>	<p>Grain-supported gravels (up to 12-cm siliceous and carbonate clasts) with low sandy matrix. Channelled or tabular massive bodies with rare horizontal bedding and imbrication. Gcm-Gh</p> <p>Grey laminated fine to coarse sands in tabular strata. Sh</p> <p>Disorganized brown gravels (up to 10-cm siliceous and carbonate clasts) with high fine-sand matrix content. Gmm</p> <p>Irregular strata made on laminated limestone with floating clasts. Lc</p> <p>Sandy matrix- or grain-supported gravels (up to 10-cm siliceous and carbonate clasts) forming lobe or channel bodies. Gmm-Gcm</p> <p>Massive sands and silts in tabular strata. Sh-Fm</p>
<p>2. Terrace T8 Ebro R. +210 m (Soriano, 1990). Early Pleistocene (Gil, Luzón, et al., 2013)</p> <p>Shallow lake and palustrine area (L)</p> <p>Alluvial fan. Cohesive gravity flow deposits (SG1)</p> <p>Fluvial system. Longitudinal bars (GB) and braided channels</p>	<p>Reddish and grey, massive or laminated mud. Fm-FI</p> <p>Matrix-supported, limestone angular boulders (up to 1 m). Gmm</p> <p>Grain-supported gravels than can be homogeneous, or show trough cross- and horizontal bedding. Subrounded, up to 15 cm, siliceous and carbonate clasts. Sandy matrix. Gcm-Gt-Gh</p> <p>Massive or laminated fine to coarse sands. Sh</p>
<p>3. Terrace T4 Gállego R. +85 m (Benito et al., 2010). Early Pleistocene (Gil Marín et al., 1998)</p> <p>Fluvial system. Braided channels (CH) and longitudinal bars (GB) with sandy bedforms and gravity deposits (SG3) the later related to karst.</p>	<p>Grain supported gravels with trough cross- or horizontal bedding. Subrounded up to 15-cm siliceous and carbonate clasts. Sandy matrix. Gt-Gh</p> <p>Disorganized gravels, sands, and silts forming very irregular bodies. Gravel with common vertical "A" axis. Gd</p> <p>Medium to coarse sands with trough cross-bedding in lenticular levels. St</p>
<p>4. T3 Ebro R. +30 m (Soriano, 1990). Late Pleistocene (Luzón et al., 2008)</p> <p>Fluvial system. Longitudinal and transverse (GB) bars with local preservation of flooded areas and local development of gravity deposits (SG3) related to karst.</p>	<p>Grain-supported gravels massive or with horizontal bedding. Subrounded to rounded, up to 20 cm, siliceous and carbonate clasts. Sandy matrix. Gcm-Gh</p> <p>Disorganized gravels, sands, and silts in very irregular bodies. Gravel with common vertical "A" axis. Gd</p> <p>Well-sorted fine to coarse sands with planar cross-bedding in cuneiform levels. Sp</p> <p>Grey massive mud in lensoid bodies. Fm</p>
<p>5. T5 Gállego R. +75 m (Benito et al., 2010). Early Pleistocene (Soriano, Alvaro, Ortega, & Hernández, 1995)</p> <p>6. T3 Ebro R. +30 m (Soriano, 1990). Late Pleistocene (Luzón et al., 2008)</p> <p>Fluvial system. Longitudinal and transverse (GB) bars with sandy bedforms.</p> <p>Shallow lake (L)</p>	<p>Gravels with trough cross- or horizontal bedding. Rounded-subrounded up to 15-cm clasts siliceous and limestone. Open framework textures to high matrix content. Gt-Gh</p> <p>Medium-coarse sands massive or laminated. Sh</p> <p>Grey massive mud in a U-shaped body. Fm</p>

Note. The different sedimentary settings that existed in every place have also been included. The acronyms correspond to those in the Miall's (1996) code.

Shear bands and mainly reverse faults with near vertical dip and variable (decimetric to metric) vertical offsets are observed in the lower gravel units (with antithetic dipping in Example 3, Figure 7c). Beds are dipping towards the areas of maximum deformation, where, generally, disorganized gravel, sand, and silt are present. In Example 4, two focuses of deformation can be observed and, in turn, in the eastern area, two U-shaped deposits developed. One of them is made in massive gravels (flexured and with shear bands) and sandy deposits. The other is in mud. In both outcrops, sandy and mud beds are thicker in the central part of the deformation structure. Unconformities are also observed (Figures 6 and 7). Finally, gravel beds of the upper units cover the structures, and only in its base, a gentle subsidence is inferred.

To summarize the evolutionary stages, the following aspects should be emphasized. In Example 3, after initial dissolution, at least two episodes of collapse can be deduced, as well as periods of slow

subsidence that caused local thickness increase, and suffusion of low-cohesive materials (see detailed evolution in Figure 7). In Example 4 (Figure 8), at least three collapse episodes can be inferred. The deformation structure located eastwards was affected by no less than two of them that subdivide the original depression. In addition, subsidence episodes in different stages are deduced (see Figure 8).

4.3 | Complex scenario: Slow subsidence and collapse

These examples (5 and 6) are in Early and Late Pleistocene sediments (see Figures 1, 9, and 10). Gravels predominate with minor sand and mud intercalations. In the central part of both examples, 5 and 6, a cylinder-shaped mudstone body is observed (see Table 1 for details). In general, these deposits correspond to longitudinal bars and braided channels, the latter being more frequent towards the top of the

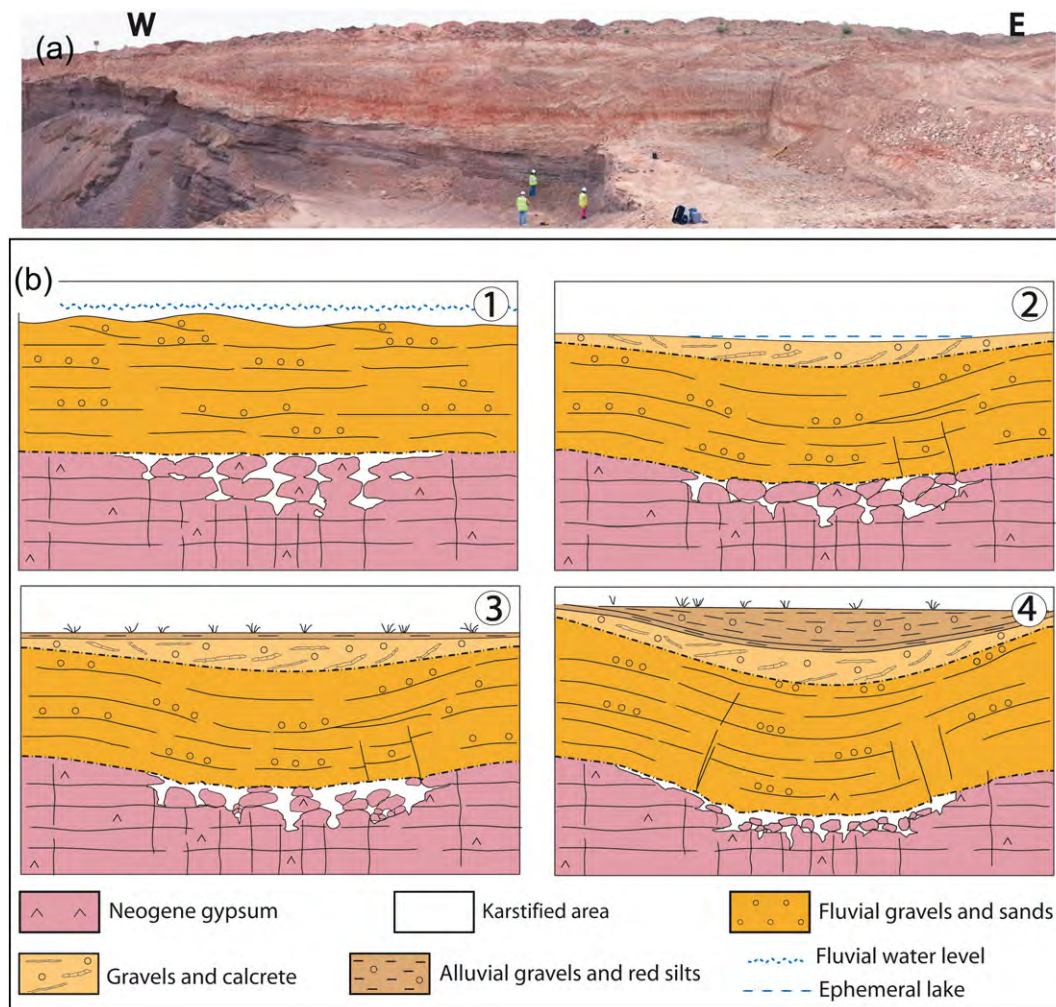


FIGURE 5 Slow subsidence case analysed (Example 1), sited SW Garrapinillos village: (a) photograph of the outcrop. (b) Evolutionary stages represented. (1) Dissolution of Neogene evaporites. Pleistocene fluvial sediments deposited on top. (2) Dissolution caused the deformation of gravel beds, development of a basin, its filling, and changes in thickness. Different calcrete levels indicate a changeable water level suggesting that different episodes of subsidence occurred. (3) Presence of a red silty level without thickness variations indicated a temporal interruption of subsidence. (4) Subsidence continued. The attenuation of deformation in the upper deposits evinces the end of subsidence processes in this site [Colour figure can be viewed at wileyonlinelibrary.com]

succession. Fining-upward cycles (gravel/sand) can be identified indicating different pulses of bar growth that, in turn, represent changes in the flow energy with time. Mudstone has been interpreted as related to lacustrine deposition (Figures 9a,c and 10).

The two deformation structures in the examples have a length of around 150 m (although only 70 m are represented in the illustration of Example 5), and both show a complex internal arrangement. Beds are dipping towards the central part of the structure. Gravel-sand cycles in the base of Case 5, representing gravel bars, increase in thickness towards the west, indicating the existence of areas with syndimentary differential subsidence.

In both examples, 5 and 6, a wide subsidence area affected by later collapses in the zones of maximum flexure is interpreted. Normal faults exist in the external area of the deformation structures. However, numerous reverse faults are observed in the central sector (Figures 9a,c and 10). The main characteristics of all these faults are high dipping, mainly NNW-SSE and also NE-SW and NW-SE striking surfaces, dipping both E and W, in Case 5, and NNE-SSW, E-W, and NW-SE surfaces in Case 6 (Figures 9b and 10b). The vertical offsets

are variable (mm to tens of m), and in some cases, two faults (normal and reverse) can converge upwards. Shear bands are also present. Noticeable increase of thickness of some levels indicates syndimentary deformation.

Moreover, in the deformation structure of Example 5, folds, erosive surfaces, beds with nearly vertical disposition, growth strata, and deformed primary sedimentary structures are also frequent. There is a collapsed area, 30 m wide, which contains in its central part another collapsed mudstone body with an almost cylindrical shape and 10 m width. These mudstones are surrounded by gravel and sand levels that belong to the older unit. They are almost vertical in the exposed basal zone of the structure with dip diminishing upwards. Dragging of gravel, sand, and mud is noticed in the base of the collapse.

In the deformation structure of Example 6, there is also a net cylindrical-shaped structure, being the western border (with gravel beds defining a progressive unconformity), more abrupt than the eastern one. In both examples described, the base of the gravel units that covers the collapsed area is slightly deformed, disappearing the deformation towards the top.

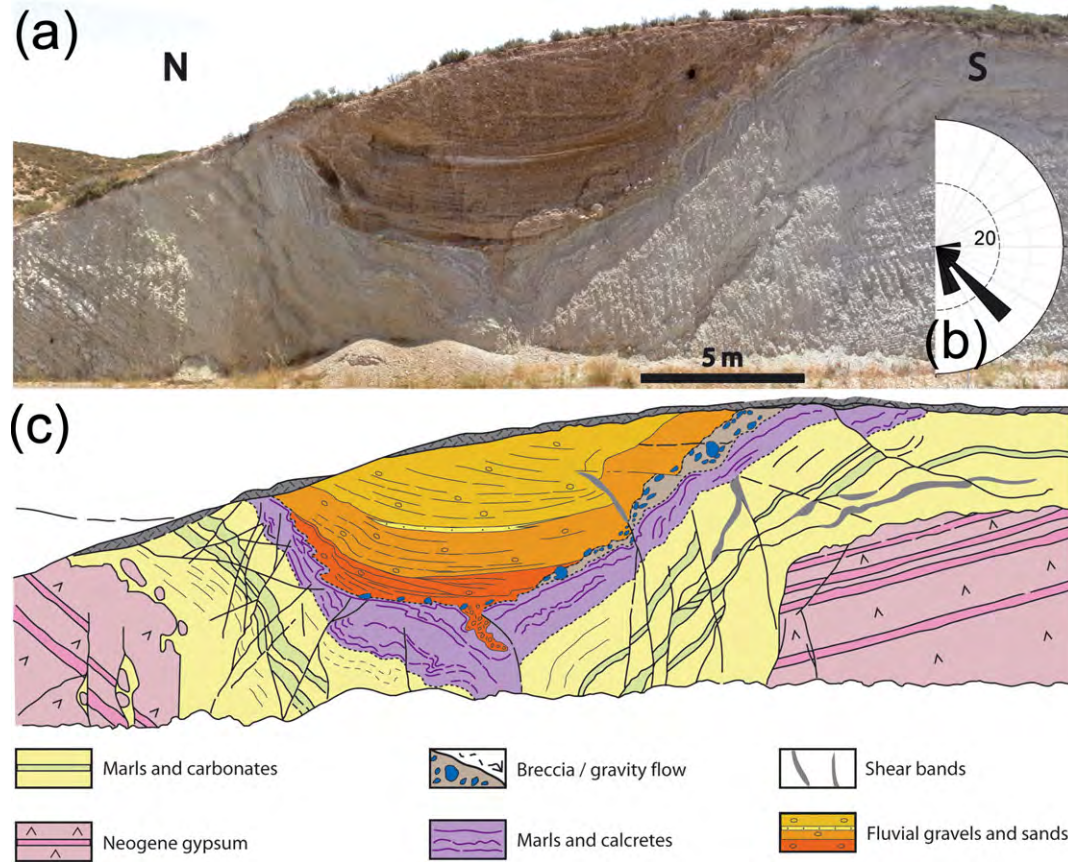


FIGURE 6 Complex case placed N of Mediana de Aragón (Example 2): (a) Field view. (b) Stereoplot of fracture orientations. (c) Cross-section. Dissolution, favoured by fractures, caused the tilting of evaporite beds. Shallow lake and palustrine areas where muds settled out and crust sedimented were generated. Later on, alluvial fan gravity flows, reworking an older pediment remains, reached the depression. Finally, fluvial deposits covered the area. The existence of shear bands, folds, and faults evinces that instability caused by dissolution and collapse continued, whereas gravel deposited and finally deformation decreased. Besides, presence of dragged gravel in the base of the structure indicates that suffosion contributed to the development of this deformation structure [Colour figure can be viewed at wileyonlinelibrary.com]

In summary, after dissolution of the Neogene evaporites, several important syndimentary subsidence episodes developed affecting the Pleistocene deposits, followed by collapses that acted repeatedly throughout time (at least in Case 5) and that favoured the establishment of a lacustrine area where mud settled out. Younger gravel levels cover and seal the whole deformation area.

4.4 | Estimation of parameters in karst paleostructures: Comparison with present-day dolines.

The geometric parameters of the 123 examples with different shapes (Table 2) were estimated: diameter and height (Figure 3) and, subsequently, the area and volume affected by karstification (Table 3). Some of them correspond to one of the described simple scenarios; meanwhile, other examples include a more complex pattern with a succession of two or three processes (Table 2). Cylindrical shapes (associated to collapse processes) are more frequently seen than cone shapes (slow subsidence). Moreover, from these observations, most of the cylinders develop associated with cones (61%). This percentage is slightly reduced (52%) when considering those collapses generated after an initial subsidence.

After all the examples were assigned to either cylindrical or cone shape, an approximation by defect of basic parameters radius and

height (with the limitations exposed in chapter 3) was measured. This permitted to compare among radius of cone and cylinder shapes, the radius of these paleoshapes with the present-day ones (inventory available in Simón et al., 1998), and, also, to obtain an estimate of the area and volume disturbed by karstification (Table 3). Comparison between the lower cones and cylinder radii shows a good correlation. A linear regression analysis of the measured pairs of radii was made (see Figure 11a) and found the straight line $y = 0.0641539 + 0.432941 x$, which fits the data with $RS = 0.661122$. In this, the length of cone radius is approximately 1.7 times the length of the cylinder one. Similar results are obtained in the relationship between cylinders and upper cones. Juxtaposition of the radii of paleostructures with data of current dolines shows right skewed unimodal distributions. Lengths in present ones are bigger than in old ones (Figure 11b). As a consequence, areas of both cones and cylinders of karst paleostructures are less than those of present-day dolines (Figure 11c). The histogram of the total volume of karst paleostructures shows an almost normal distribution (Figure 11d). The mean of the total volume affected by karst is 8110.161 m^3 , and most of the cases have a volume between 10^2 and 10^3 m^3 . In Figure 11d is also represented, with thinner bars, the number of cases identified as cones and cylinders for each interval of volume. In general, the histograms are coincident with that of

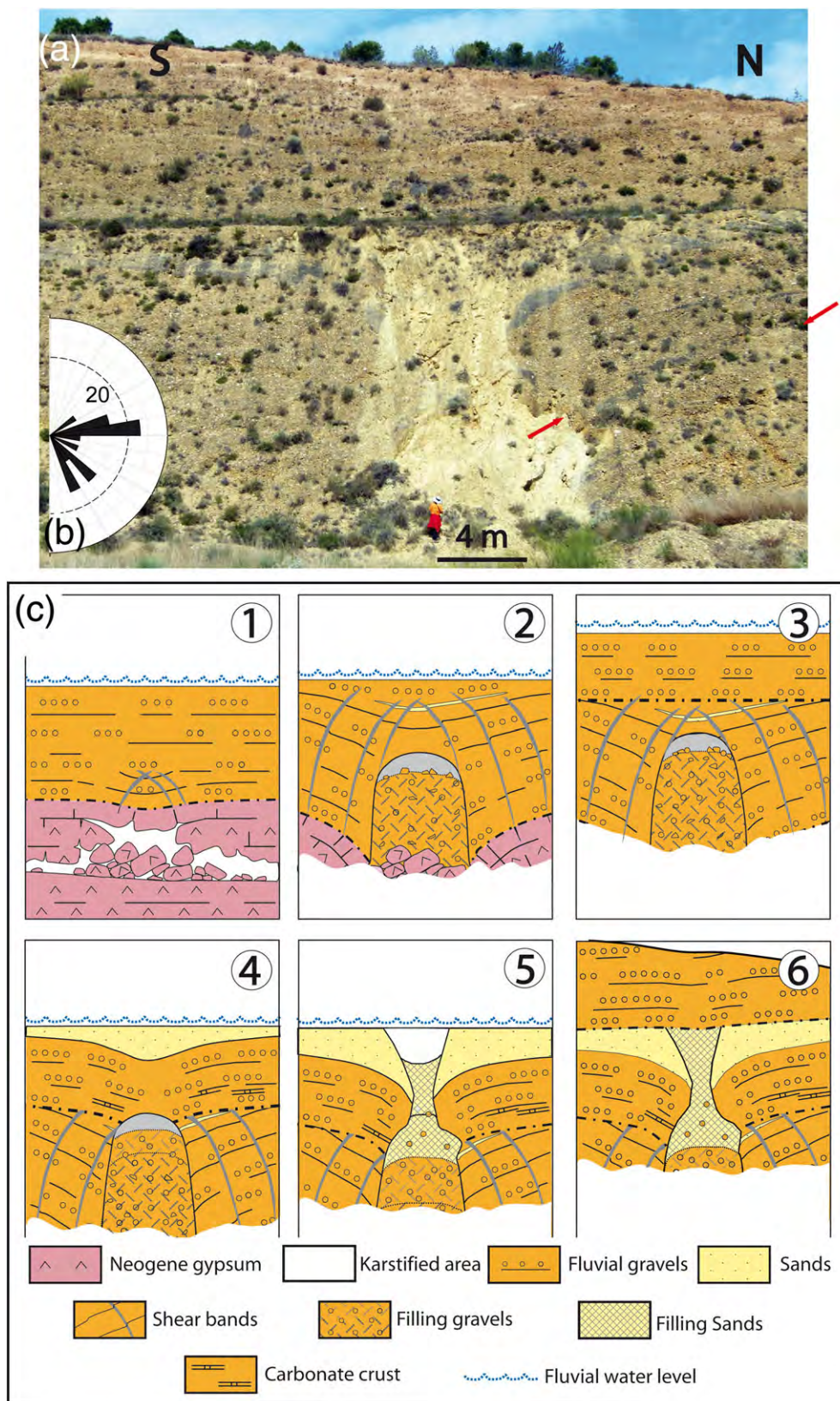


FIGURE 7 Collapse observed in Example 3, located N of Zaragoza: (a) picture of the outcrop. The arrows mark unconformity between Units 1 and 2. (b) Stereoplot of the fracture orientations. (c) Evolutionary model is in sketches 1 to 6. (1) Dissolution of Neogene evaporites generated conduits and cavities, and deformation of beds towards these voids. Early Pleistocene fluvial sediments deposited over the evaporites were slightly affected by such processes. (2) Progression of the stress upwards resulted in the collapse of the clastic sediments, dipping of beds, and generation of shear bands. (3) Sedimentation of younger gravels took place unconformably. (4) The continuous growth of the cavity upwards caused dipping of gravel beds and syndepositional increase in thickness of silty-sandy levels. (5) Connection of the collapse with the silty-sandy level, caused dragging and a funnel shape. (6) The upper gravel unit was deposited being the basal levels still affected by subsidence. Subsidence ended and no more deformation is observed in this site [Colour figure can be viewed at wileyonlinelibrary.com]

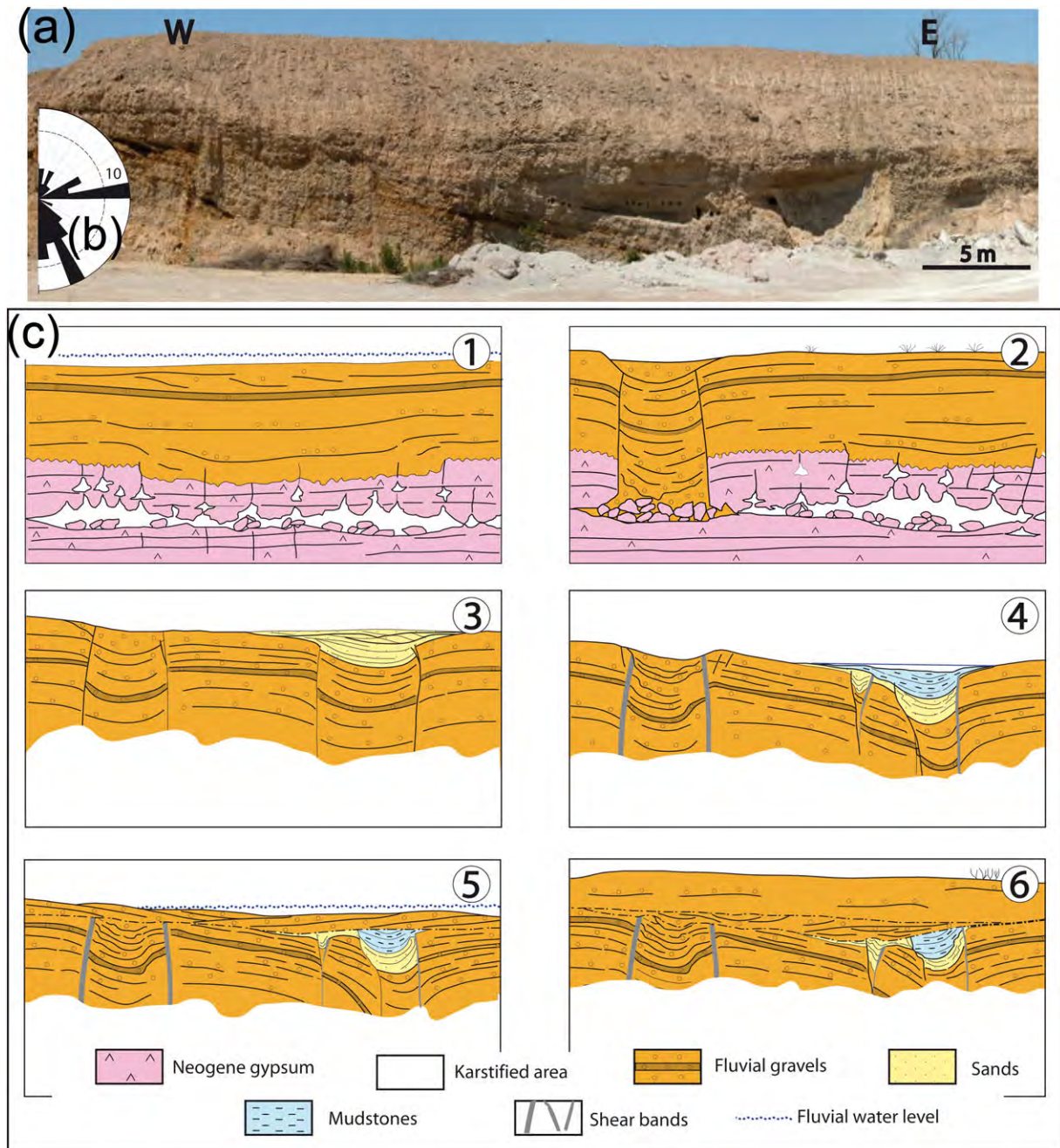


FIGURE 8 Collapses situated SW Garrapinillos Village (Example 4): (a) photograph of the outcrop. (b) Stereoplot of the fracture orientations. (c) Sketches 1 to 6 show the evolutionary stages inferred to this deformation structure. (1) A wide zone with Neogene evaporites would be affected by dissolution where slight differences in depth of the main levels dissolved existed. Sedimentation of fluvial braided deposits started. Dissolution of evaporites caused subsidence in Pleistocene beds. (2) The western karstified area collapsed and propagated upwards affecting Pleistocene fluvial deposits. (3) Dissolution continued and a second collapse produced eastwards. Sands deposited in a fluvial channel. (4) Differences in dissolution drove into the generation of two subsidence foci inside of the eastern original one, where muds settled out in a slow subsiding pond. (5 and 6) Fluvial sedimentation continued, basal levels still reflected subsidence [Colour figure can be viewed at wileyonlinelibrary.com]

total volume, except for the case of the upper cone, in which the maximum number of depressions is in the interval of 10^3 to 10^4 m³.

5 | DISCUSSION

The study carried out concerning diverse deformation structures in Pleistocene deposits of the central Ebro Basin suggests that their genesis is related to karstification of Neogene evaporites. This dissolution

was not homogeneous. Generally, Neogene layers are slightly deformed (Figure 4c). However, locally, deformation is important (see Figure 4d), favoured by the presence of both highly soluble levels (Cooper, 1986; Cooper & Waltham, 1999; Ford & Williams, 2007; Guerrero et al., 2013; Gutierrez et al., 2008; White, 1988; Figure 4a) and/or fractures, which connect evaporite beds located at different depths (Figure 4b). Preferential paths for ground water circulation are created (Abelson et al., 2006; Closson, 2005; Gil, Pepe, et al., 2013; Jassim, Jibril, & Numan, 1997).

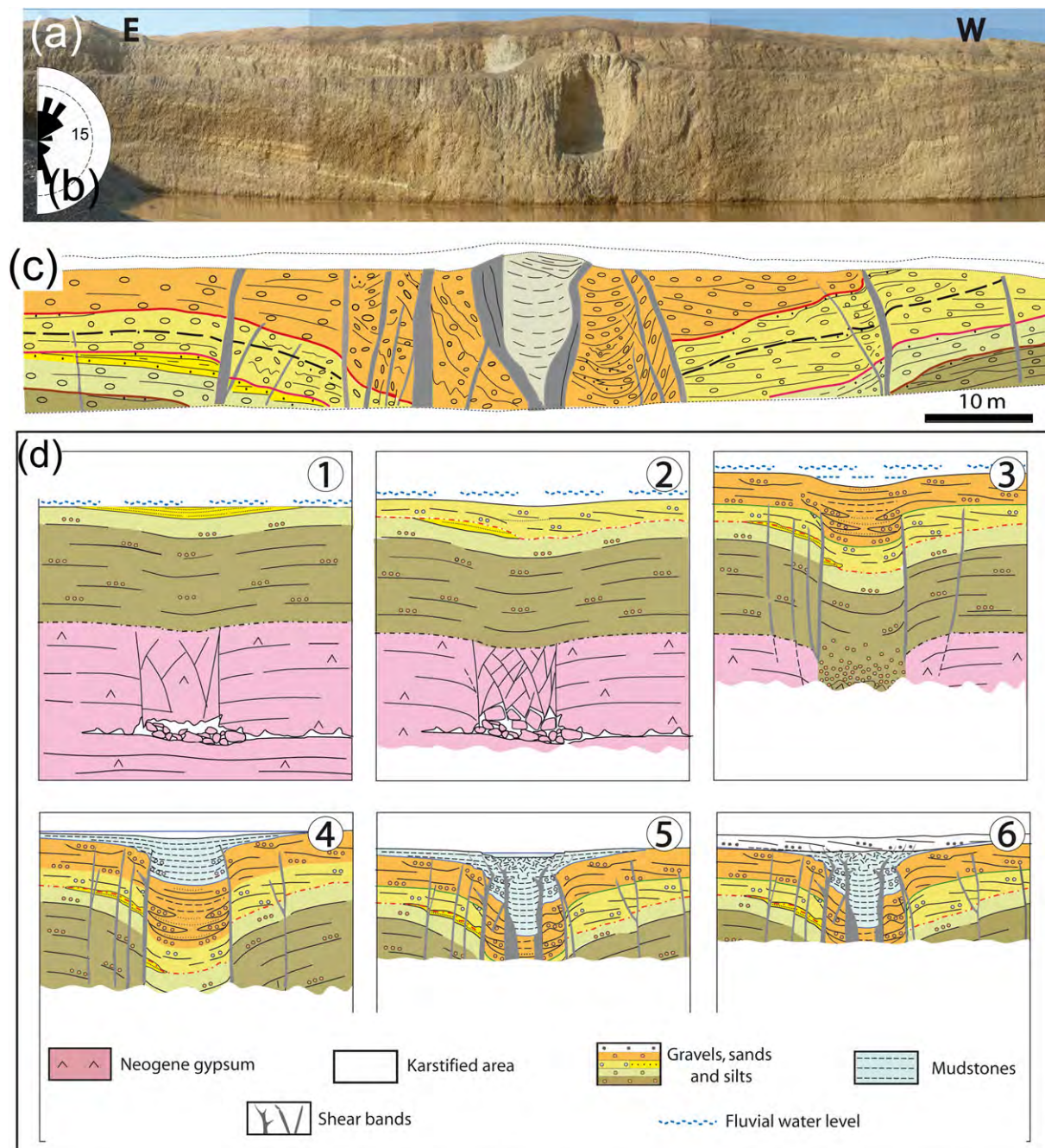


FIGURE 9 Slow subsidence and later sudden-collapse case analysed in Example 5, W of Zuera: (a) field view. (b) Stereoplot of fracture orientations. (c) Cross-section of the present view. (d) Evolutionary episodes are represented in simplified cross-sections named 1 to 6. (1) Dissolution and deformation of the Neogene evaporite substratum generated. Fluvial sedimentation started and syndimentary subsidence occurred as the increase in thickness of some of the Pleistocene levels indicates. (2) Subsequent partial erosion of Pleistocene beds by younger deposits, asymmetry in the subsidence zone and increase in thickness of beds indicates that dissolution continued. (3) Fractures and faults generated in Pleistocene deposits. Later on, major dissolution in the flexure zone favoured the generation of a collapse (4). A lacustrine area developed where muds settled (5). A new collapse that affects the central area of the first one took place, causing the sinking of mudstones. Important shear bands affecting gravel and sand developed (6). Younger gravel levels deposited [Colour figure can be viewed at wileyonlinelibrary.com]

The sedimentological characteristics of the Pleistocene deposits indicate that most of the studied examples generated in a gravel-dominated braided fluvial system and in lateral alluvial fans (Gil, Luzón, et al., 2013; Luzón et al., 2008; Pérez et al., 2011). Subsidence in the central Ebro Basin has confirmed to be syndimentary with Quaternary deposition, as is demonstrated by the existence of growth strata, tilting, unconformities (evincing that subsidence is not a continuous process throughout the time), and fractures (their main trends are

coherent with those dominant in the main stress field in this area of the Ebro Basin) observed.

When a long section across a basin shape deformation structure is accessible, changes in the distribution of fault types are frequently observed, with the normal ones dominating far from the sinking centre and reverse ones with opposite dips in the inner areas of the basin structure (Figures 9 and 10). This variation was also observed in experimental models by Ge and Jackson (1998), which considered that the



FIGURE 10 Slow subsidence and later sudden-collapse case analysed in Example 6, SW Garrapinillos Village. Dissolution of Neogene caused subsidence in fluvial deposits and development of fractures and faults. A collapse is developed in the central area, where mud settled out. Deformation is attenuated to the top and new gravel beds cover the previous feature [Colour figure can be viewed at wileyonlinelibrary.com]

TABLE 2 Number of simple and complex processes observed in this study

1 (lower cone)	2 (cylinder)	3 (upper cone)
66	110	36
8	43	4
36		10
21		

accommodation space explains the opposite dip of faults, whereas Simón et al. (2014) attribute it to differences in cohesion of the subsiding material in relation to the bounding one. In addition, this evinces that the deformation is maximum in the central area, but the range of deformation extends radially in tens of metres.

Whether dissolution has followed preferential beds (intrastratal dissolution), numerous conduits could have developed generating sagging by flexure of the overlying beds. As a result, synform structures of variable size originate (Figures 7c and 9d). When deformation progresses upwards, basins (dolines) can be generated at the surface. In

addition, in zones where the water table coincides or is immediately below the sedimentary surface, calcretes, ponds, or lakes (not common in fluvial environments) can generate with mud settling (Figures 5, 6, and 12b). Whether subsidence continues, mud flowed because of its low viscosity and folds with axial plane dipping towards the sinking centre generated (see Figure 6a,c). When sedimentation is active, no morphological evidences of the existence of a subsidence zone can be seen at the surface (Ford & Williams, 2007). However, as demonstrated by Gil, Luzón, et al. (2013), in the sections where palaeokarst is exposed, thickened channels can be observed. Moreover, because dissolution is not homogeneous in the whole affected area, one (Figures 5, 6, and 12a) or several centres (Figure 12b) of dissolution may be generated (Gil et al., 2012), and even smaller subsidence nuclei appear inside a bigger depression (see Pueyo-Anchuela et al., 2014). Slow subsidence can be the main process detected (Figures 5 and 6) or play a more secondary role (Figures 9 and 10). It also was widely observed in other studies (Cooper & Waltham, 1999; Doğan & Özel, 2005; Gil, Luzón, et al., 2013; Guerrero et al., 2013; Hyatt, Wilkes, & Jacobs, 1999; Luzón et al., 2008; Simón et al., 2014).

In addition to slow subsidence, cavities grow upwards by failure of the uppermost layers. A tension dome can be created in the rock above the passage, being the ceiling subjected to elastic sagging (Andrejchuk & Klimchouk, 2002; Parise, 2008; Parise & Lollino, 2008; Lollino, Martimucci, & Parise, 2013; Figure 7) and the walls to increasing stress. All of this generates diverse downwards-concave tensile fractures resulting in a cupola shape (Simón et al., 2014). Successive collapses

TABLE 3 Minimum, mean, and maximum values of radius, area, and volume obtained in Paleodoline and Recent dolines

	Paleodoline					Recent dolines		
	1	2	3	1 or 3	1, 2, or 3	1 or 3	2	1, 2, or 3
No. of data	66	110	36	78	123	185	58	231
Radius (m)	2.0 21.8 87.5	0.45 6.607 41.5	2.25 11.949 32.5	2.0 19.599 87.5	0.45 14.047 87.5	2.5 64.506 225.0	1.0 16.841 55.0	1.0 54.702 225.0
Area (m ²)	12.566 2,349.412 24,052.819	0.636 302.421 5,410.608	15.904 632.301 3,318.307	12.566 2,008.574 24,052.819	0.636 1,330.533 24,052.819	19.635 15,425.207 141,371.669	3.142 1,072.854 8,796.459	3.142 12,493.619 141,371.669
Volume (m ³)	2.094 6,551.373 128,281.7	0.954 4,644.89 108,212.159	1.856 1,159.425 14,379.365	6.512 11,264.574 141,461.031	0.954 8,008.628 216,351.29			

Note. 1, 2, and 3 indicate lower cone, cylinder, and upper cone, respectively.

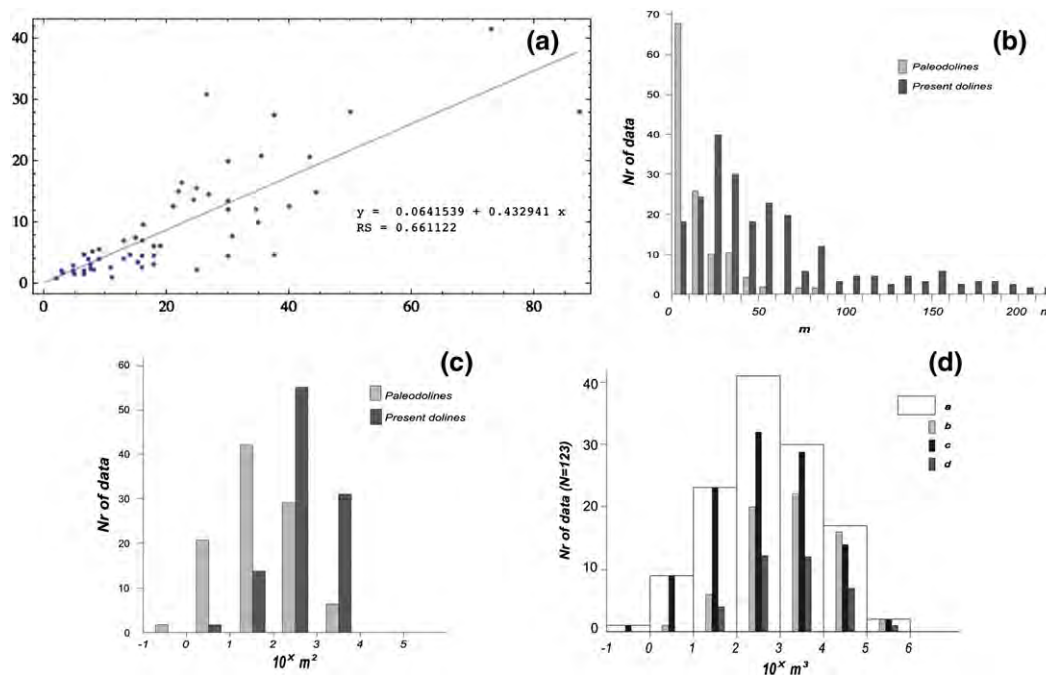


FIGURE 11 (a) Linear regression between radii of lower cone and cylinder showed. (b,c) Histograms of radii and area comparison between paleodolines and present dolines. (d) Histogram of total volume of paleodolines (a). Thinner bars (b, c, and d) represent the number of cases for lower cones, cylinders, and upper cones, respectively, for each interval of volume

can occur (Figure 7c), and the breakdown pile of fragments can be accumulated at the floor of the cavity (Klimchouk & Andrejchuk, 2002). Presence of a resistant bed can restrain the cavity growing up and favour its lateral development (de Waele & Parise, 2013; Klimchouk, 2013), as occurred in relation to the first collapse of example Number 3 reflected in Figure 7. Deformation structures as sagging, antithetic reverse faults, and shear bands are frequently observed (Figure 12c). This type of structures is also described in experimental models (Ge & Jackson, 1998). In presence of groundwater, whether the upwards-migrating void reaches a silty-sandy level, processes as liquefaction or piping dominate, and, consequently, a cone or funnel shape develops (Klimchouk & Andrejchuk, 2002) as evidenced in Figure 7. When the upward propagation of collapses reaches the surface, dolines with steep slopes are generated, and even within large collapsed areas, new dolines can appear related with its border (Figure 8). In the presence of water, the collapsed zones can be flooded and mud settle out (Figures 8, 9, and 10). Growth strata and gravity flow processes are related to the collapse boundaries (Figures 8 and 10). Recurrence of collapses in the same place can be facilitated by the existence of previous joints and faults, as Simón et al. (2014) pointed out, and by the progressive dissolution of the breakdown pile of evaporite blocks.

Moreover, it is frequent to find that slow and fast subsidence acted throughout time at the same location, that is, a succession of processes was produced. In the example in Figure 6, both processes were deduced, but the most conspicuous examples are those represented in Figures 9 and 10, where wide subsidence zones are cut by collapses (with great height) in their central areas, and, finally, another subsidence area developed. In these cases, the initial subsidence area concentrates more water that will be directed to the deeper zone increasing dissolution (Williams, 1983). Furthermore, subsidence can

generate new fractures in the area of maximum flexure, and later on, these condition the development of the collapse superimposed to the previous deformation structure (Andrejchuk & Klimchouk, 2002). The main trends in the deformation structures described in the previous examples are coincident with tectonic ones, contributing to the important vertical displacement suffered by these deposits (estimated in tens of metres). In Example 5, there are also two collapses, one inside the other, showing a concentric disposition (Figure 9). In Examples 5 and 6, final slow subsidence with thickness increase of deposits and development of unconformities is inferred. This will have originated by progression of dissolution, compaction of materials and so forth. In analogue models of alluvial dolines (Soriano & Simón, 1997), only collapses take place at the surface in the final stages of evolution. However, collapse and suffosion can be active in the subsoil. These authors suggested that the natural development of dolines results at the end in collapse dolines, and indicate that the other situations are transitional stages to this one. Probably, the anisotropic behaviour of both the detrital cover and the evaporite conditions (a) the type and degree of participation of processes involved and (b) the transitional stage until a more stable level is reached. On the other hand, it seems logical that as much time as the same subsidence area was active, with unchanging conditions, more complexity in the behaviour of the detrital cover will be found.

As described previously, alternating episodes of mainly slow and fast subsidence processes developed in the past in the Ebro Basin affecting the Pleistocene deposits. The sequence of acting processes reveals a high degree of complexity. The six detailed examples studied, plus the more than one hundred in which diverse parameters were measured, indicate that no variations in those processes have been detected, independently of the age of the analysed deposits. Dominance of collapses and the examples with succession of processes

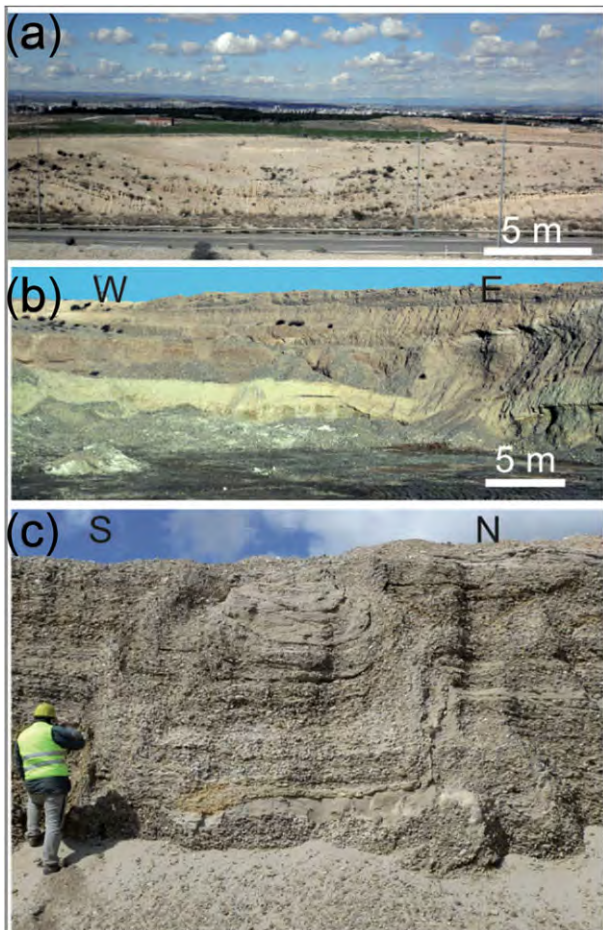


FIGURE 12 Deformation structures in Quaternary deposits: (a) slow subsidence structure with basin morphology, S of Zaragoza. (b) Variation in thickness of mud levels indicates the presence of two basins; S of Alagón. (c) Collapse structure with vault morphology sited SW Fuentes de Ebro [Colour figure can be viewed at wileyonlinelibrary.com]

(being very frequent collapses inside the slow subsidence basins) were observed (Table 2). Consequently, it can be assumed that this study not only provides information about the behaviour of karst in the past in the studied area, but also it can be a warning to present-day karst development. Today, an active mantled karst exists in the central Ebro Basin, mainly evidenced by the presence of profusely studied dolines (see Section 2). In this way, active dolines and depressions containing small dolines (subsidence dolines and mainly collapse dolines) have been profusely described in this area (Galve et al., 2009; Pueyo-Anchuela et al., 2015; Soriano & Simón, 1995) being quite similar to the paleostructures analysed in the previous examples. This is also the case in other regions in the world (Ford, 1997; Iovine, Parise, & Trocino, 2010; Nicod, 2006).

Some authors (Gutiérrez et al., 2014; Waltham et al., 2005) consider that subsidence dolines developed under a soil cover are a major geohazard related to karst, especially when human activities interfere with this process. Additionally, a lot of alluvial dolines are inherited. Quaternary levels close to Zaragoza city constitute a very populated area, and consequently, karst hazard increases. In such conditions, maintaining the equilibrium between urban expansion,

economic development, and environmental sustainability is a complex task (Lamelas, 2007).

Thus, a better knowledge of the succession of processes acting in the evolution of karst landforms can help to better delimit hazard areas and to be used in urban planning. For example, this study demonstrates that some dolines considered “inactive” could be reactivated, as indicated by the presence of unconformities in the analysed sediments due to natural causes but also when, for instance, human activities fill depressions with low cohesive materials that are exposed to later suffosion and subsidence. Besides, as has been revealed in this paper, processes that control the formation of dolines can change with time (for example, after slow subsidence, collapses can develop) with the subsequent involved hazard when this possibility has not been considered, and vice versa, fast subsidence can be followed by slow one, which affects a wider area. Moreover, the present surficial morphology of dolines is not necessarily representative of the processes that have generated them. As an example, the paleostructure depicted in Figure 6 was mainly created by slow subsidence, but the direct access to a deeper zone reveals that collapse and suffosion worked in its development. A wrong interpretation about the genetic process related to present dolines can cause important problems especially in high-density populated areas.

On the other hand, the estimation of direct parameters, such as diameter, indicates higher values for slow subsidence (1.7 times) than for collapse shapes. The comparison of both paleokarst and present-day karst depressions shows bigger values for the current ones (Table 3 and Figure 11b). This can be governed by the different observation conditions, limited outcrops in the paleodolines, and coalescence, scale of aerial photographs, filling, of the smaller ones, and so forth in the present dolines. As a result, indirect parameters present again these differences (Figure 11c,d). The main values of the volume of sediments involved in paleoforms are of the order of 10^3 m^3 . Considering those divergences between old and present-day forms parameters, most likely the main values of volume for current dolines would be of the order of 10^4 m^3 . In any case, this estimation can be valuable in land-use planning and in a better determination of economic costs.

In addition, the reactivation of palaeokarst can take place, as Ford and Williams (2007) pointed out in mantled karst in Canada or Horwitz and Smith (2003) in Florida. In the Ebro Basin, climate is semiarid, but human activities (old irrigation practices that flood the fields) provide supplies to groundwater recharge estimated to be 20 times those by natural precipitation (Soriano et al., 2012). In other cases, intense pumping (as in quarries) can contribute to modify the ground water level. These are examples that imply subsequent increase in risk.

To this end, a better knowledge of the succession of diverse karst processes obtained from the study of old deformation structures generated by karst can be useful not only to delimitate the present hazard zones mitigating the exposure to this geohazard but also to be aware that even evolution of slow subsidence dolines can modify their development and evolution with the following increase in hazard in the affected area. Alerting the authorities is basic, as they have to look after the safety of citizens (Zhou, Yan, Chen, & Zhang, 2016).

6 | CONCLUSIONS

In the Pleistocene deposits of the central Ebro Basin, numerous deformation features have been generated as consequence of dissolution in the underlying Neogene evaporites. Many of these deformation structures are synsedimentary with Quaternary deposits, as the characteristics of such deposits and of the analysed structures indicate.

The detailed study of these deformation structures shows more collapse than slow subsidence processes. A complex development with, usually, diverse processes, affecting both the evaporite beds and the detrital cover, cooperates in their genesis. Some of them can be detected, thanks to the existence of peculiarities in the sedimentary architecture.

This research allowed the determination of diverse karst evolutionary stages affecting the Pleistocene detrital deposits. This has a direct application to the study of present dolines as it indicates that (a) in some occasions, the present surficial morphology of dolines is not necessarily representative of the real processes that generated them, (b) dolines considered inactive can be reactivated, (c) processes that condition the formation of dolines in a specific location can change with time (for instance, after slow subsidence, collapse can develop) with the subsequent involved hazard when this possibility has not been evaluated, (d) an approximation to size of parameters, its relation in size, and also, the volume of materials affected by karstification. In addition, it seems that collapse is a very profuse stage in natural evolution of dolines and that can be developed even after episodes of slow subsidence. This type of evolution also implies a subsequent increase of risk, mainly in urban zones. These changes in evolutionary patterns must be considered by the authorities in order to avoid influence of both natural and man-made hazards in the region, to achieve a better land use and, consequently, to provide safety conditions to inhabitants of the affected areas.

ACKNOWLEDGEMENTS

The interesting suggestions and comments of the editor and referee1 help to improve the quality of this work. This work has been partially supported by the Geotransfer research group (Gobierno de Aragón and FEDER Aragón 2014-2020).

ORCID

María Asunción Soriano  <http://orcid.org/0000-0002-2842-517X>

REFERENCES

- Abelson, M., Yechieli, Y., Crouvi, O., Baer, G., Wachs, D., Bein, A., & Shtivelman, V. (2006). Evolution of the Dead Sea sinkholes. *Geological Society of America Special Paper*, 401, 241–253. [https://doi.org/10.1130/2006.2401\(16\)](https://doi.org/10.1130/2006.2401(16))
- Andrejchuk, V., & Klimchouk, A. (2002). Mechanisms of karst breakdown formation in the gypsum karst of the fore-Ural region, Russia (from observations in the Kungurskaja cave). *International Journal of Speleology*, 31, 89–114. <https://doi.org/10.5038/1827-806X.31.1.5>
- Arche, A., Evans, G., & Clavell, E. (2010). Some considerations on the initiation of the present SE Ebro river drainage system: Post- or pre-Messinian? *Journal of Iberian Geology*, 36, 73–85.
- Arlegui, L. E., & Simón, J. L. (2000). Fracturación y campos de esfuerzos en el Cuaternario del sector central de la Cuenca del Ebro. *Cuaternario y Geomorfología*, 14, 11–20.
- Arlegui, L. E., & Simón, J. L. (2001). Geometry and distribution of regional joint sets in a non-homogeneous stress field: Case study in the Ebro Basin (Spain). *Journal of Structural Geology*, 23, 297–313. [https://doi.org/10.1016/S0191-8141\(00\)00097-3](https://doi.org/10.1016/S0191-8141(00)00097-3)
- Arlegui, L. E., & Soriano, M. A. (2003). An example of a comparison between thematic mapper and radar images in the central Ebro Basin. *International Journal of Remote Sensing*, 24, 457–474. <https://doi.org/10.1080/01431160304996>
- Beck, B. F. (1984). *Sinkholes: Their geology, engineering and environmental impact*. Rotterdam: Balkema.
- Beck, B. F., & Pearson, F. M. (1995). *Karst geohazards: Engineering and environmental problems in karst terrane*. Rotterdam: Balkema.
- Benito, G., Pérez-González, A., Gutierrez, F., & Machado, M. J. (1998). River response to quaternary subsidence due to evaporite solution (Gállego River, Ebro Basin, Spain). *Geomorphology*, 22, 243–263. [https://doi.org/10.1016/S0169-555X\(97\)00088-3](https://doi.org/10.1016/S0169-555X(97)00088-3)
- Benito, G., Sancho, C., Peña, J. L., Machado, M. J., & Rhodes, E. (2010). Large-scale karst subsidence and accelerated fluvial aggradation during MIS6 in NE Spain: Climatic and paleohydrological implications. *Quaternary Science Reviews*, 29, 2694–2704. <https://doi.org/10.1016/j.quascirev.2010.06.020>
- Bosák, P. (1989). An introduction to Karst-related mineral deposits. In P. Bosák, D. C. Ford, J. Glazek, & I. Horáček (Eds.), *Paleokarst. A systematic and regional review* (pp. 367–376). Praha: Elsevier and Academia.
- Bosák, P., Ford, D. C., & Glazek, J. (1989). Terminology. In P. Bosák, D. C. Ford, J. Glazek, & I. Horáček (Eds.), *Paleokarst. A systematic and regional review* (pp. 25–32). Praha: Elsevier and Academia.
- Closson, D. (2005). Structural control of sinkholes and subsidence hazards along the Jordanian Dead Sea coast. *Environmental Geology*, 47, 290–301. <https://doi.org/10.1007/s00254-004-1155-4>
- Columbu, A., Waele, J. D., Forti, P., Montagna, P., Picotti, V., Pons-Branchu, E., ... Drysdale, R. (2015). Gypsum caves as indicators of climate-driven river incision and aggradation in a rapidly uplifting region. *Geology*, 43, 539–542. <https://doi.org/10.1130/G36595.1>
- Confederación Hidrográfica del Ebro. (2017). Base de inventario de puntos de agua. <http://www.chebro.es/contenido.visualizar.do?idContenido=2887%26idMenu=3061>
- Cooper, A. H. (1986). Subsidence and foundering of strata caused by the dissolution of Permian gypsum in the Ripon and Bedale areas, North Yorkshire. *Geological Society, London, Special Publications*, 22, 127–139. <https://doi.org/10.1144/GSL.SP.1986.022.01.11>
- Cooper, A. H., & Waltham, A. C. (1999). Subsidence caused by gypsum dissolution at Ripon, North Yorkshire. *Quarterly Journal of Engineering Geology*, 32, 305–310. <https://doi.org/10.1144/GSL.QJEG.1999.032.P4.01>
- de Waele, J., & Parise, M. (2013). Discussion on the article “coastal and inland karst morphologies driven by sea level stands: A GIS based method for their evaluation” by Canora, F., Fidelibus, D. and Spilotro, G. *Earth Surface Processes and Landforms*, 38, 902–907. <https://doi.org/10.1002/esp.3412>
- De Waele, J., Piccini, L., Columbu, A., Madonia, G., Vattano, M., Calligaris, C., ... Forti, P. (2017). Evaporite karst in Italy: A review. *International Journal of Speleology*, 46, 137–168. <https://doi.org/10.5038/1827-806X.46.2.2107>
- Decarlis, A., & Lualdi, A. (2008). Late Triassic-Early Jurassic Paleokarst from the Ligurian Alps and its geological significance (Siderolitico Auct., Ligurian Briançonnais domain). *Swiss Journal Geosciences*, 101, 579–593. <https://doi.org/10.1007/s00015-008-1302-0>
- Doğan, U., & Özel, S. (2005). Gypsum karst and its evolution east of Hafik (Sivas, Turkey). *Geomorphology*, 71, 373–388. <https://doi.org/10.1016/j.geomorph.2005.04.009>
- Eliassen, A., & Talbot, M. R. (2005). Solution-collapse breccias of the Minkinfjellet and Wordiekammen Formations, Central Spitsbergen, Svalbard: A large gypsum palaeokarst system. *Sedimentology*, 52, 775–794. <https://doi.org/10.1111/j.1365-3091.2005.00731.x>

- Eraso, A. (1989). Paleokarst in civil engineering. In P. Bosák, D. C. Ford, J. Glazek, & I. Horáček (Eds.), *Paleokarst. A systematic and regional review* (pp. 549–557). Praha: Elsevier and Academia.
- Ershova, V., Prokopiev, A., Khudoleya, A., & Fefilova, L. (2012). Deposits in paleokarst caverns as indicators of carboniferous Paleogeographic environments in the northeastern part of the Siberian platform. *Doklady Akademii Nauk*, 442, 511–515. <https://doi.org/10.1134/S1028334X12020031>
- Esnaola, J. M., & Leyva, F. (1995). *Mapa geológico y memoria explicativa de Pedrola*. Mapa geológico de España. (1:50.000)
- Evans, J. E., & Reed, J. M. (2007). Integrated loessite-paleokarst depositional system, early Pennsylvanian Molas Formation, Paradox Basin, southwestern Colorado, USA. *Sedimentary Geology*, 195, 161–181. <https://doi.org/10.1016/j.sedgeo.2006.07.010>
- Fei, T., Qiang, J., Xinbian, L., Yuhong, L., Likuan, Z., Songqing, Z., ... Naigui, L. (2016). Multi-layered ordovician paleokarst reservoir detection and spatial delineation: A case study in the Tahe oil field, Tarim Basin, Western China. *Marine and Petroleum Geology*, 69, 53–73. <https://doi.org/10.1016/j.marpetgeo.2015.10.015>
- Ford, D. C. (1997). Principal features of evaporite karst in Canada. *Carbonate & Evaporite*, 12, 15–23. <https://doi.org/10.1007/BF03175798>
- Ford, D. C., & Williams, P. W. (2007). *Karst geomorphology and hydrology*. Chichester: John Wiley & Sons.
- Galve, J. P., Gutierrez-Santolalla, F., Lucha, P., Bonachea, J., Remondo, J., Cendrero, A., ... Sanchez, J. A. (2009). Sinkholes in the salt-bearing evaporite karst of the Ebro River valley upstream of Zaragoza city (NE Spain) geomorphological mapping and analysis as a basis for risk management. *Geomorphology*, 108, 145–158. <https://doi.org/10.1016/j.geomorph.2008.12.018>
- García-Castellanos, D. J., Vergés, J. M., Gaspar-Escribano, J., & Cloetingh, S. (2003). Interplay between tectonics, climate and fluvial transport during the Cenozoic evolution of the Ebro Basin (NE Iberia). *Journal of Geophysical Research*, 108(B7), 2347. <https://doi.org/10.1029/2002JB002073>
- Ge, H., & Jackson, M. P. (1998). Physical modelling of structures formed by salt withdrawal: Implications for deformation caused by salt dissolution. *American Association of Petroleum Geologists Bulletin*, 82, 228–250.
- Gil, H., Luzón, A., Soriano, M. A., Casado, I., Pérez, A., Yuste, A., ... Pocoví, A. (2013). Stratigraphic architecture of alluvial-aeolian systems developed on active karst terrains: An early Pleistocene example from the Ebro Basin (NE Spain). *Sedimentary Geology*, 296, 122–141. <https://doi.org/10.1016/j.sedgeo.2013.08.009>
- Gil, H., Luzón, A., Soriano, M. A., Pueyo, O., Pocoví, A., & Pérez, A. (2012). Ejemplos de formas paleokársticas y depósitos asociados en los materiales detríticos de terraza del río Ebro. *Geogaceta*, 52, 97–100. (in Spanish)
- Gil, H., Pepe, M., Soriano, M. A., Parise, M., Pocoví, A., Luzón, A., ... Basso, A. (2013). Sviluppo ed evoluzione di sprofondamenti in rocce solubili: un confronto tra il carso coperto del Bacino dell'Ebro (Spagna) e la Penisola Salentina (Italia). *Memorie Descrittive Della Carta geologica d'Italia, XCIII*, 215–238. (in Italian)
- Gil Marín, C., Esnaola Gómez, J.M., Marqués, L. & Herranz, J.M. (1998). Mapa geológico y memoria explicativa de Zaragoza. Mapa geológico de España (1:50.000).
- Guerrero, J., Gutierrez, F., & Galve, J. P. (2013). Large depressions, thickened terraces, and gravitational deformation in the Ebro River valley (Zaragoza area, NE Spain) evidence of glauberite and halite interstratal karstification. *Geomorphology*, 196, 162–176. <https://doi.org/10.1016/j.geomorph.2012.06.024>
- Guerrero, J., Gutierrez, F., & Lucha, P. (2004). Paleosubsidence and active subsidence due to evaporite dissolution in the Zaragoza area (Huerva River valley, NE Spain): Processes, spatial distribution and protection measures for transport routes. *Engineering Geology*, 72, 309–329. <https://doi.org/10.1016/j.enggeo.2003.10.002>
- Guerrero, J., Gutierrez, F., & Lucha, P. (2008). Impact of halite dissolution subsidence on Quaternary fluvial terrace development: Case study of the Huerva River, Ebro Basin, NE Spain. *Geomorphology*, 100, 164–179. <https://doi.org/10.1016/j.geomorph.2007.04.040>
- Gutierrez-Santolalla, F., Gutiérrez-Elorza, M., Marín, C., Maldonado, C., & Younger, P. L. (2005). Subsidence hazard avoidance based on geomorphological mapping in the Ebro River valley mantled evaporite karst terrain (NE Spain). *Environmental Geology*, 48, 370–383. <https://doi.org/10.1007/s00254-005-1281-7>
- Gutiérrez, F., Guerrero, J., & Lucha, P. (2008). A genetic classification of sinkholes illustrated from evaporite paleokarst exposures in Spain. *Environmental Geology*, 53, 993–1006. <https://doi.org/10.1007/s00254-007-0727-5>
- Gutiérrez, F., Parise, M., de Waele, J., & Jourde, J. (2014). Review on natural and human-induced geohazards and impacts in karst. *Earth-Science Reviews*, 138, 61–88. <https://doi.org/10.1016/j.earscirev.2014.08.002>
- Horwitz, M., & Smith, T. (2003). Characteristics of stable and reactivated in-filled paleo-karst features in west-Central Florida. In B. Beck (Ed.), *Sinkholes and the engineering and environmental impacts of karst* (pp. 50–60). Reston, VA, USA: American Society of Civil Engineers. [doi.org/10.1061/40698\(2003\)4](https://doi.org/10.1061/40698(2003)4)
- Hyatt, J., Wilkes, H., & Jacobs, P. (1999). Spatial relationship between new and old sinkholes in covered karst, Albany, Georgia, USA. In B. F. Beck, A. J. Pettit, & J. G. Herring (Eds.), *Hydrogeology and engineering geology of sinkholes and karst. Proceedings of the seventh multidisciplinary conference on sinkholes and the engineering and environmental impacts of karst* (pp. 37–44). Rotterdam: Balkema.
- Iovine, G., Parise, M., & Trocino, A. (2010). Breakdown mechanisms in gypsum caves of southern Italy, and the related effects at the surface. *Zeitschrift für Geomorphologie*, 54, 153–178. <https://doi.org/10.1127/0372-8854/2010/0054S2-0009>
- Jassim, S. Z., Jibril, A., & Numan, N. M. S. (1997). Gypsum karstification in the Middle Miocene Fatha Formation, Mosul area, northern Iraq. *Geomorphology*, 18, 137–149. [https://doi.org/10.1016/S0169-555X\(96\)00018-9](https://doi.org/10.1016/S0169-555X(96)00018-9)
- Julián Andrés, A., & Chueca Cía, J. (1998). Acumulaciones fluviales en la depresión del Ebro: Valoración de la validez de una secuencia general. *Geographical*, 36, 67–82.
- Khalaf, F. I. (2011). Occurrence of diagenetic pseudobreccias within the paleokarst zone of the upper Dammam Formation in Kuwait, Arabian gulf. *Arabian Journal of Geosciences*, 4, 703–718. <https://doi.org/10.1007/s12517-009-0070-0>
- Klimchouk, A., & Andrejchuk, V. (2002). Karst breakdown mechanisms from observations in the gypsum caves of the western Ukraine: Implications for subsidence hazard assessment. *International Journal of Speleology*, 31, 55–88. <https://doi.org/10.5038/1827-806X.31.1.4>
- Klimchouk A.B. (2013). Evolution of intrastratal karst and caves in gypsum. In: Shroder, J., Frumkin, A., (Eds.), *Treatise on geomorphology*. Academic Press, San Diego, CA, vol. 6, Karst Geomorphology, pp. 438–450. [doi:10.1016/B978-0-12-374739-6.00123-8](https://doi.org/10.1016/B978-0-12-374739-6.00123-8)
- Lamelas, M. T., Marinoni, O., Hoppe, A., & de la Riva, J. (2008). Doline probability map using logistic regression and GIS technology in the central Ebro Basin (Spain). *Environmental Geology*, 54, 963–977. <https://doi.org/10.1007/s00254-007-0895-3>
- Lamelas, T. (2007). *Geo-resources and geo-hazards in the context of a sustainable development in the periphery of urban areas, exemplary of a part of the Ebro Basin in the surroundings of Zaragoza (Spain)*. Tesis Darmstadt University of Technology and Universidad de Zaragoza.
- Land, L., & Asanidze, L. (2015). Rollalong resistivity surveys reveal karstic paleotopography developed on near-surface gypsum bedrock, 14th Sinkhole Conference, 366–370.
- Liesa, C. L., & Simón, J. L. (2009). Evolution of intraplate stress fields under multiple remote compressions; the case of the Iberian chain (NE Spain). *Tectonophysics*, 474, 144–159. <https://doi.org/10.1016/j.tecto.2009.02.002>

- Lollino, P., Martimucci, V., & Parise, M. (2013). Geological survey and numerical modeling of the potential failure mechanisms of underground caves. *Geosystem Engineering*, 16, 100–112.
- Luzón, A., Pérez, A., Pocoví, A., Soriano, M. A., Gil, H., Rodríguez-López, J. P., & Simón, J. L. (2011). Sedimentary record related to the evolution of Quaternary dolines in the central Ebro Basin (Spain). In C. Arenas, L. Pomar, & F. Colombo (Eds.), *Pre-Meeting field trips guidebook, 28th IAS meeting* (pp. 151–198). Zaragoza, 7:199–226: (Sociedad Geológica de España) Geo-Guías.
- Luzón, A., Pérez, A., Soriano, M. A., & Pocoví, A. (2008). Sedimentary record of Pleistocene paleodoline evolution in the Ebro basin (NE Spain). *Sedimentary Geology*, 205, 1–13. <https://doi.org/10.1016/j.sedgeo.2008.01.004>
- Luzón, A., Rodríguez-López, J. P., Pérez, A., Soriano, M. A., Gil, H., & Pocoví, A. (2012). Karst subsidence as a control on the accumulation and preservation of aeolian deposits a Pleistocene example from a proglacial outwash setting, Ebro Basin, Spain. *Sedimentology*, 59, 2199–2225. <https://doi.org/10.1111/j.1365-3091.2012.01341.x>
- Mancini, F., Stecchi, F., Zanni, M., & Gabbianelli, G. (2009). Monitoring ground subsidence induced by salt mining in the city of Tuzla (Bosnia and Herzegovina). *Environmental Geology*, 58, 381–389. <https://doi.org/10.1007/s00254-008-1597-1>
- Marqués, L.A., Santos, J.A., Esnaola, J.M., & Gil, C. (1998). Mapa geológico y memoria explicativa de Fuentes de Ebro. Mapa geológico de España (1:50.000).
- Miall, A. D. (1996). *The geology of fluvial deposits. Sedimentary Facies, Basin Analysis, and Petroleum Geology*. Berlin: Springer-Verlag.
- Min, M. Z., & Mao, S. L. (2002). The Saqisan mine paleokarst uranium deposit, South China. *Ore Geology Reviews*, 19, 79–93. [https://doi.org/10.1016/S0169-1368\(00\)00010-X](https://doi.org/10.1016/S0169-1368(00)00010-X)
- Muñoz, A., Arenas, C., González, A., Luzón, A., Pardo, G., Pérez, A., & Villena, J. (2002). Ebro Basin (northeastern Spain). In W. Gibbons, & T. Moreno (Eds.), *The geology of Spain* (pp. 301–309). London: Geological Society of London.
- Nicod, J. (2006). Lakes in gypsum karst: Some examples in alpine and Mediterranean countries. *Acta Carsologica*, 35, 69–78. <https://doi.org/10.3986/ac.v35i1.244>
- Pardo, G., Arenas, C., González, A., Luzón, A., Muñoz, A., Pérez, A., ... Villena, J. (2004). In J. A. Vera, & IGME and Sociedad Geológica de España (Eds.), *La Cuenca del Ebro* (pp. 533–539). Madrid: Geología de España.
- Parise, M. (2008). Rock failures in karst. In: Cheng, Z., Zhang, J., Li, Z., Wu, F. and Ho, K. (eds), *Landslides and engineered slopes*. Proc. 10th International Symposium on Landslides, Xi'an (China), 1, 275–280.
- Parise, M., & Lollino, P. (2008). A preliminary analysis of failure mechanisms in karst and man-made underground caves in Southern Italy. *Geomorphology*, 134, 132–143. <https://doi.org/10.1016/j.geomorph.2011.06.008>
- Parise M., Ravbar N., Živanovic V., Mikszewski A., Kresic N., Mádl-Szo'nyí J. & Kukuric N. (2015) Hazards in karst and managing water resources quality. Chapter 17 in: Z. Stevanovic (ed.), *Karst aquifers—Characterization and engineering*. Professional Practice in Earth Sciences. Doi: 10.1007/978-3-319-12850-4_17, Springer, 601–687.
- Pérez, A., Pueyo, O., Gil, H., Soriano, M. A., Luzón, A., & Pocoví, A. (2011). Deltas de gravas asociados a depósitos fluviales pleistocenos afectados por colapsos kársticos y su estudio con ayuda técnicas GPR (Cuenca del Ebro, NE España). *Geogaceta*, 50, 117–120. (in Spanish)
- Pueyo-Anchuela, Ó., Casas, A. M., Soriano, M. A., & Pocoví, A. (2010). A geophysical survey routine for the detection of doline areas in the surroundings of Zaragoza (NE Spain). *Engineering Geology*, 114, 382–396. <https://doi.org/10.1016/j.enggeo.2010.05.015>
- Pueyo-Anchuela, Ó., López Julián, P., Casas Sainz, A. M., Liesa, C. L., Pocoví Juan, A., Ramajo Cordero, J., & Pérez Benedicto, J. A. (2015). Three dimensional characterization of complex mantled karst structures. Decision making and engineering solutions applied to a road overlying evaporite rocks in the Ebro Basin (Spain). *Engineering Geology*, 193, 158–172. <https://doi.org/10.1016/j.enggeo.2015.04.022>
- Pueyo-Anchuela, O., Luzón, A., Gil-Garbi, H., Pérez, A., Pocoví, A., & Soriano, M. A. (2014). Combination of electromagnetic, geophysical methods and sedimentological studies for the development of 3D models in alluvial sediments affected by karst (Ebro Basin, NE Spain). *Journal of Applied Geophysics*, 102, 81–95. <https://doi.org/10.1016/j.jappgeo.2014.01.002>
- Quirantes, J. (1978). Estudio sedimentológico y estratigráfico del Terciario Continental de los Monegros. In *Instituto Fernando el Católico, (CSIC)*. Diputación Provincial de Zaragoza: Zaragoza.
- Rodríguez-Aranda, J. P., Calvo, J. P., & Sanz-Montero, E. (2002). Lower Miocene gypsum palaeokarst in the Madrid Basin (central Spain): Dissolution diagenesis, morphological relics and karst end-products. *Sedimentology*, 49(6), 1385–1400. <https://doi.org/10.1046/j.1365-3091.2002.00504.x>
- Silva, P. G., López Recio, M., Cuartero, F., Baena, J., Tapias, F., Manzano, I., ... Roquero, E. (2012). Contexto geomorfológico y principales rasgos tecnológicos de nuevos yacimientos del Pleistoceno Medio y Superior en el Valle Inferior del Manzanares (Madrid, España). *Estudios Geológicos*, 68, 57–89. <https://doi.org/10.3989/egeol.40336.133>
- Simón, J.L., Soriano, M.A., Arlegui, L., & Caballero, J. (1998). Estudio de riesgos de hundimientos kársticos en el corredor de la carretera de Logroño, <http://www.zaragoza.es/contenidos/urbanismo/pgouz/memoria/anejos/anejo03/anejo032.pdf>.
- Simón, J. L., Soriano, M. A., Pérez, A., Luzón, A., Pocoví, A., & Gil, H. (2014). Interacting tectonic faulting, karst subsidence, diapirism and continental sedimentation in Pleistocene deposits of the central Ebro Basin (Spain). *Geological Magazine*, 151, 1115–1134. <https://doi.org/10.1017/S0016756814000156>
- Smith, G.M., & Goodknight, C.S. (2005). Quaternary salt dissolution in the Moab-Spanish Valley, UT; pleistocene and holocene evidence. Abstracts with programs, Geological Society of America, Colorado, United States. pp. 36–37.
- Soriano, C., Alvaro, M., Ortega, I., & Hernández, A. (1995). Mapa geológico y memoria explicativa de Zuera. Mapa geológico de España (1:50.000).
- Soriano, M. A. (1990). *Geomorfología del sector centromeridional de la Depresión del Ebro*. Zaragoza: Institución Fernando el Católico.
- Soriano, M. A., Luzón, A., Yuste, A., Pocoví, A., Pérez, A., Simón, J. L., & Gil, H. (2012). Quaternary alluvial sinkholes: Record of environmental conditions of karst development, examples from the Ebro Basin, Spain. *Journal of Cave and Karst Studies*, 74, 173–185. <https://doi.org/10.4311/2011JCKS0201>
- Soriano, M. A., & Simón, J. L. (1995). Alluvial dolines in the entral Ebro Basin, Spain: A spatial and developmental hazard analysis. *Geomorphology*, 11, 295–309. [https://doi.org/10.1016/0169-555X\(94\)00066-Z](https://doi.org/10.1016/0169-555X(94)00066-Z)
- Soriano, M. A., & Simón, J. L. (1997). Analogue models of alluvial doline development. *Géologie Méditerranéenne*, 24, 3–13.
- Soriano, M. A., & Simón, J. L. (2002). Subsidence rates and urban damages in alluvial dolines of the Central Ebro basin (NE Spain). *Environmental Geology*, 42, 476–484. <https://doi.org/10.1007/s00254-001-0508-5>
- Waltham, T. (2008). Sinkhole hazard case histories in karst terrains. *Quarterly Journal of Engineering Geology and Hydrogeology*, 41, 291–300. <https://doi.org/10.1144/1470-9236/07-211>
- Waltham, T., Bell, F., & Culshaw, M. (2005). *Sinkholes and subsidence: Karst and cavernous rocks in engineering and construction*. Berlin: Springer.
- Warren, K. J. (2006). *Evaporites Sediments, Resources and Hydrocarbons*. Berlin: Springer.
- White, E. L., & White, W. B. (1969). Processes of cavern breakdown. *Bulletin of the National Speleological Society of America*, 31, 83–96.

- White, W. (1988). *Geomorphology and hydrology of karst terrains*. New York: Oxford University Press.
- Williams, P. (2003). Dolines. In J. Gunn (Ed.), *Encyclopedia of caves and karst science* (pp. 304–310). New York: Fitzroy Dearborn.
- Williams, P. W. (1983). The role of the subcutaneous zone in karst hydrology. *Journal of Hydrology*, 61, 45–67. [https://doi.org/10.1016/0022-1694\(83\)90234-2](https://doi.org/10.1016/0022-1694(83)90234-2)
- Zhao, W., Shen, A., Qiao, Z., Zheng, J. & Wang, X (2014). Carbonate karst reservoirs of the Tarim Basin, northwest China: Types, features, origins, and implications for the hydrocarbon exploration: Interpretation. *Journal of subsurface characterization*, 2, SF 65-SF90. doi: 10.1190/INT-2013-0177.1
- Zhou, G., Yan, H., Chen, K., & Zhang, R. (2016). Spatial analysis for susceptibility of second-time karst sinkholes: A case study of Jili Village in Guangxi, China. *Computers & Geosciences*, 89, 144–160. <https://doi.org/10.1016/j.cageo.2016.02.001>

How to cite this article: Soriano MA, Pocoví A, Gil H, Pérez A, Luzón A, Marazuela MÁ. Some evolutionary patterns of palaeokarst developed in Pleistocene deposits (Ebro Basin, NE Spain): Improving geohazard awareness in present-day karst. *Geological Journal*. 2018;1–18. <https://doi.org/10.1002/gj.3181>